Hydrol. Earth Syst. Sci., 30, 7177–7195, 2026
https://doi.org/10.5194/hess-30-7177-2026
© Author(s) 2026. This work is distributed under
the Creative Commons Attribution 4.0 License.

Hydrology and Earth System Sciences
Open Access
EGU

Characterizing runoff response to rainfall in permafrost catchments and its implications for hydrological and biogeochemical fluxes in a warming climate

Cansu Culha[1,2], Sarah Godsey[3], Shawn Chartrand[4], Melissa Lafrenière[5], James P. McNamara[6], and James W. Kirchner[7,8]

[1]Department of Earth, Ocean and Atmospheric Sciences, University of British Columbia, Vancouver, BC V6T 1Z4, Canada
[2]PermaC Land & Environment Inc., Vancouver, BC V6K 1E2, Canada
[3]Department of Geosciences, Idaho State University, Pocatello, ID 83209, USA
[4]Department of Geography, Simon Fraser University, Burnaby, BC V5A 1S6, Canada
[5]Department of Geography and Planning, Queen's University, Kingston, ON K7L 3N6, Canada
[6]Department of Geosciences, Boise State University, Boise, ID 83725, USA
[7]Department of Environmental Systems Science, ETH Zürich, Zürich, 8092, Switzerland
[8]Swiss Federal Research Institute WSL, Birmensdorf, 8903, Switzerland

Correspondence: Cansu Culha (cansu.culha@gmail.com) and James W. Kirchner (kirchner@env.eth.ch)

Received: 2 September 2025 – Discussion started: 17 October 2025
Revised: 25 September 2026 – Accepted: 29 September 2026 – Published: 20 November 2026

Abstract. Understanding how Arctic catchments respond to rainfall is critical for anticipating hydrological and biogeochemical effects of a warming climate. We use ensemble rainfall-runoff analysis (ERRA) to identify how runoff response to rainfall varies with meteorological, subsurface, and geomorphic conditions across three permafrost catchments: Upper Kuparuk (Alaska) and the Goose and Ptarmigan catchments (Cape Bounty, Nunavut, Canadian High Arctic). ERRA enables us to quantify event-scale runoff responses to rainfall using high-resolution, multi-year hydrometeorological datasets, and test how variations in rainfall intensity, thaw depth, antecedent effective wetness, and active layer detachments (ALDs) affect runoff behavior. At Upper Kuparuk, our results show that peak runoff response increases by more than five-fold in response to increases in antecedent streamflow (a proxy for antecedent effective wetness), and is also higher in summers with higher average precipitation. By contrast, at the same catchment, warmer winters and springs are associated with reduced runoff sensitivity to rainfall. Furthermore, a paired watershed comparison shows that streamflow and riverine fluxes of dissolved solids, suspended sediment, and particulate organic carbon are more readily mobilized by rainfall inputs when ALDs are present. Considered together, these findings highlight the difficulty in generalizing climate-driven runoff trends in permafrost regions subject to competing and interacting controls, such as precipitation intensity, storage capacity and permafrost stability. Our findings offer a more nuanced alternative to broad classifications of Arctic landscapes as "drying" or "wetting" under climate change.

1 Introduction

Catchments underlain by continuous permafrost (land frozen for at least two consecutive years; van Everdingen, 1998; Woo et al., 2000) are often largely impermeable, and thus can rapidly transport rain, snowmelt, and meltwaters from ground ice downstream (Woo and Steer, 1982; McNamara et al., 1999; Levy et al., 2011). With climate warming, the active layer (the surface layer that freezes and thaws seasonally) is expected to become thicker (Jorgenson et al., 2010; Levy et al., 2011; Wang et al., 2021a, b; Painter et al., 2023), thereby altering subsurface flow patterns, increasing near-surface groundwater volumes, and increasing water storage capacity (McNamara et al., 1997; Smith et al., 2007;

Walvoord and Striegl, 2007; St. Jacques and Sauchyn, 2009; Velicogna et al., 2012; Frampton and Destouni, 2015; Walvoord and Kurylyk, 2016; Eschenfelder et al., 2026). These hydrologic changes are not only expected to affect streamflow dynamics, but also to exert strong controls on the mobilization and transport of dissolved and particulate carbon and other materials, particularly during short-lived rainfall events (Stieglitz et al., 2003; Spence et al., 2015; DeBeer et al., 2016; Crowther et al., 2016; Toohey et al., 2016; Coch et al., 2018; Beel et al., 2020, 2021). To better understand how climate change may affect solute and sediment transport in Arctic streams, we investigate how streamflow and material flux response to rainfall are shaped by precipitation intensity and ambient conditions. Climate change projections suggest that Arctic precipitation will increase in coming decades, with increasing prevalence of rainfall relative to snowfall (Bintanja and Andry, 2017; Bintanja et al., 2020; Bieniek et al., 2022). However, it is unclear whether these changes will lead to higher peak flows following rainfall events, and thus flashier flood responses, or whether these effects will be damped by deeper thaw and increases in subsurface storage capacity and groundwater flow volumes.

Understanding how climatic shifts may change the timing and magnitude of peak streamflow following a rainfall event is challenging due to confounding effects of changing precipitation patterns, increasing storage, and potentially accelerating landscape erosion. While deeper thaw is generally expected to increase subsurface storage capacity (Stähli et al., 1999; Stieglitz et al., 2003; Scherler et al., 2010; Painter et al., 2023; Qin et al., 2025), observations from continuous permafrost environments suggest that the active layer may still function as a relatively weak hydrologic buffer, permitting rapid runoff responses to both intense rainfall and prolonged dry periods (Kane et al., 2008). Consequently, it remains unclear whether climate-driven increases in active-layer thickness will systematically reduce runoff intensity. Moreover, observational evidence is often confounded by other environmental controls. For example, prolonged dry periods can independently reduce runoff responses by increasing available storage, whereas sustained rainfall or snow and ice melt may increase catchment saturation and hydrologic connectivity, making streamflow more responsive to rainfall inputs (Stieglitz et al., 2003; Kurylyk and Watanabe, 2013). Likewise, landscape change associated with active-layer erosion may alter surface and subsurface flow pathways and reduce storage capacity, thereby accelerating runoff responses (Beel et al., 2020). Because these processes can simultaneously confound, amplify, or mask one another, quantifying their individual contributions remains a significant but necessary challenge.

Ground-based observations and modeling are commonly used to understand controls on streamflow dynamics in permafrost landscapes, each with distinct strengths and limitations. Long-term ground-based studies have provided some of the most detailed hydrologic, chemical, and biogeochemical observations available for permafrost catchments. These studies have documented strong seasonal controls on runoff generation, solute transport, and flowpath activation associated with active layer development and changing hydrologic connectivity (e.g., McNamara et al., 1998; Kane et al., 2000; Stieglitz et al., 2003; Shogren et al., 2019, 2022; Beel et al., 2021; Grewal et al., 2025). Runoff and material flux responses in Arctic catchments reflect complex interactions among precipitation timing, antecedent effective wetness, thaw depth, and spatially variable subsurface permeability, often resulting in nonlinear or near-chemostatic concentration–discharge behavior (e.g., Tank et al., 2020; Shogren et al., 2019, 2022; Grewal et al., 2025). Conceptual and process-based frameworks developed in tundra and permafrost environments likewise emphasize the importance of vertical and lateral contrasts in hydraulic conductivity and threshold-driven hydrologic connectivity in shaping runoff response (e.g., Quinton and Marsh, 1999; Quinton et al., 2000; Kokelj et al., 2013, 2017).

Despite these advances, collecting long-term, high-frequency observational data in Arctic environments remains challenging and costly, and many existing analyses focus on seasonal or annual responses rather than event-scale rainfall–runoff dynamics. Simulation models have advanced substantially in their ability to represent coupled cold-region processes and to project hydrologic change in permafrost landscapes, including recent pan-Arctic runoff simulations and integrated surface–subsurface thermal hydrology models (e.g., Stieglitz et al., 2003; Painter et al., 2013, 2016; Jan et al., 2020; Evans et al., 2020; Rawlins et al., 2021; Rawlins and Karmalka, 2024). However, quantitative constraints on how permeability, hydraulic gradients, and effective subsurface storage evolve at event timescales in response to rainfall and snow/ice melt remain limited (Kurylyk and Watanabe, 2013; Favaro and Lamoureux,, 2014; Walvoord and Kurylyk, 2016; Chen et al., 2022). These gaps motivate the use of data-driven approaches that can directly quantify nonlinear and nonstationary runoff responses to rainfall at event-scales.

Furthermore, while many studies have focused on how permafrost thaw alters annual or seasonal material export from Arctic catchments (e.g., Beel et al., 2020; Tank et al., 2023), far less is known about the general response characteristics of carbon and sediment to rainfall on timescales of hours to days after averaging across the diverse hydrometeorological conditions under which individual events occur. Yet a generalized description for each catchment at event scales is critical, as short-lived increases in runoff can disproportionately control the timing, magnitude, and form (dissolved versus particulate) of material export. Quantifying how rainfall can shape these event-driven fluxes is therefore essential for linking hydrologic change to biogeochemical export in permafrost landscapes.

Building on this motivation, our study characterizes how summer runoff responses to rainfall in permafrost landscapes regulate event-scale hydrologic conditions that govern mate-

rial mobilization. We characterize and quantify how summer runoff in response to rainfall in landscapes underlain by permafrost is affected by precipitation intensity and antecedent effective wetness on timescales of hours to days, as well as precipitation and average temperatures during preceding seasons, the seasonal development of the active layer, and the erosion of the land surface. In this paper, "runoff" is understood to mean streamflow normalized by catchment area, potentially including both overland and subsurface flow. Our analysis makes use of multi-year time series data of runoff, precipitation, temperature and material flux from the Upper Kuparuk River near Toolik Lake, Alaska, and the Goose and Ptarmigan catchments of Melville Island, Nunavut, Canada. We quantify the lagged response of runoff to rainfall, and examine how it varies with meteorological forcing and ambient catchment characteristics, yielding insight into the factors that amplify or dampen runoff response to precipitation. Because streamflow is one way by which sediment and solutes are mobilized and exported from Arctic catchments, we extend this framework to material flux data from the Melville catchments to quantify lagged material flux runoff to rainfall.

Historically, runoff response to precipitation has often been characterized using unit hydrographs that capture the lagged response to precipitation events (Beven, 2012). However, unit hydrograph approaches are not well suited for quantifying the influence of factors such as rainfall intensity and antecedent effective wetness, because unit hydrographs typically assume runoff response is linear (i.e., proportional to precipitation) and stationary (i.e., independent of the ambient conditions when rain falls), whereas observed runoff response is often nonlinear and nonstationary. Instead, we apply ensemble rainfall-runoff analysis (ERRA: Kirchner, 2024), a data-driven, model-independent method for quantifying nonlinear and nonstationary rainfall-runoff relationships directly from time series data, and extend this framework to quantify event-scale material flux responses to rainfall.

Using ERRA, we characterize the influence of processes modulating runoff response in permafrost landscapes on timescales of hours, months, and years. The Upper Kuparuk (Fig. 1a) and Cape Bounty (Goose and Ptarmigan, Fig. 1b) catchments provide multiple years of meteorologic, soil and streamflow data publicly available at 1 h resolution, making them ideal for this analysis. Furthermore, these catchments are relatively free of the confounding effects of glacial melt inputs (Kane et al., 2000). Additionally, the Ptarmigan catchment has two active layer detachments (ALDs; Lamoureux and Lafrenière, 2009), which are mass movements that initiate downslope sliding of the seasonally thawed active layer at the frozen-unfrozen interface, exposing the surface of the permafrost (the frost table) to the atmosphere (Paquette et al., 2020). Characterizing the role of ALDs in runoff response to rainfall provides a unique opportunity to understand how these thermoerosional features can impact runoff as permafrost destabilizes (Fig. 1c), which is critical because ALDs (Beel et al., 2018, 2020, 2021; Lafrenière and Lamoureux, 2019) and other thermoerosional features occur widely in ice-rich and thermokarst-susceptible terrain (e.g., Gooseff et al., 2009; Kokelj et al., 2023, 2026) . They can exert disproportionate geomorphic and hydrologic influence and their areal extent and frequency have increased in many regions in recent decades, consistent with more extreme weather events and permafrost degradation (Bowden et al., 2008; Gooseff et al., 2009; Liljedahl et al., 2016; Biskaborn et al., 2019). Overall, the Upper Kuparuk, Goose and Ptarmigan catchments serve as natural laboratories for investigating the influence of meteorologic activity, active layer thaw depth and active layer detachment on permafrost runoff response.

2 Catchment descriptions and existing data

2.1 Upper Kuparuk

The Upper Kuparuk River (Fig. 1a) originates at 1464 m a.s.l. in the Brooks Range of northern Alaska and drains 142 km^2 at its outlet (68°38′24.5″ N and 149°24′23.4″ W, 778 m a.s.l.), where precipitation and streamflow have been recorded at hourly intervals since 2003 (Arp et al., 2017; Kane et al., 2021). Here we use data from 2005 and 2007–2017, since these years have a higher fraction of logged precipitation and streamflow data (see Fig. S1a in the Supplement). Hourly measurements are available for stream discharge (Onset Hobo U20 stage records, calibrated with biweekly discharge measurements using a Teledyne StreamPro Acoustic Doppler Current Profiler), precipitation (Texas Electronics TR-525M tipping bucket rain gauge), air temperature (Vaisala HMP45C temperature sensor mounted at 1 m above ground), and soil temperature (Campbell Scientific CS615 and CS616 soil temperature probes). As ERRA integrates runoff responses across many input events (e.g., hourly), these high-frequency measurements enable characterization of integrated catchment behavior with reduced sensitivity to occasional uncertainty.

Unlike larger Arctic river basins that may receive extensive glacial melt or aufeis inputs, the Upper Kuparuk headwater catchment has limited active water sources (primarily precipitation and permafrost thaw) following spring snowmelt (McNamara et al., 1998). The catchment typically starts its flow season in May and discharges almost all of its snowmelt by June (Kane et al., 2000), after which roughly two-thirds of summer precipitation leaves the catchment as streamflow (McNamara et al., 1998), implying that evapotranspiration, temporary soil storage, and/or deeper soil storage are relatively small components of the water balance. During peak thaw, continuous permafrost extends to 250–600 m depth with an active layer of approximately 50 cm (e.g., Nelson et al., 1997; Kane et al., 2008; Arp et al., 2015), precluding deep groundwater contributions to summer streamflow,

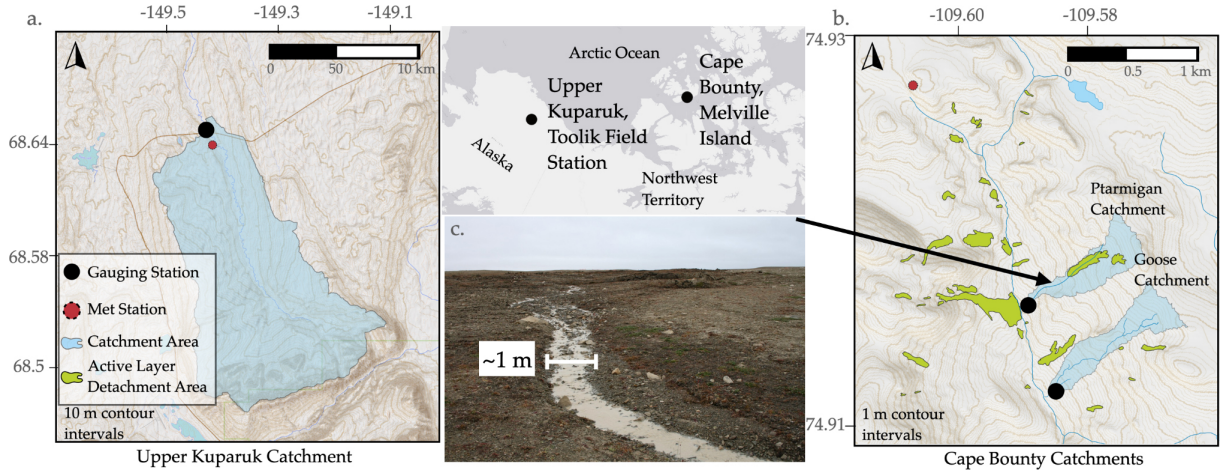


Figure 1. Maps of the permafrost catchments that inform this study. **(a)** Upper Kuparuk Catchment map near Toolik Field Station, northern Alaska; **(b)** Cape Bounty map with Ptarmigan and Goose catchments; **(c)** A photo of enhanced runoff from an active layer detachment (ALD) at Ptarmigan (stream is approximately 1 m wide). Maps are generated using ArcticDEM data (Porter et al., 2018).

which is instead derived from precipitation, melting permafrost and active-layer ice, and shallow subsurface flow. Following spring snowmelt, the limited number of active water sources allows for a focused analysis of the impacts of rainfall and thaw on permafrost hydrology.

2.2 Cape Bounty: Ptarmigan and Goose catchments

We also analyze two headwater catchments in the West River watershed of Cape Bounty Arctic Watershed Observatory (CBAWO), Melville Island in the Canadian High Arctic (74°54′ N, 109°35′ W; Fig. 1b). Similar to the Upper Kuparuk, the Cape Bounty catchments have multiple years of measurements taken daily or sub-daily between 2006 and 2018. However, data collection was not as consistent as at the Upper Kuparuk, limiting the types of analyses that are possible (Fig. S1b–c).

We focus on two adjacent headwater catchments at Cape Bounty: Goose (0.18 km^2) and Ptarmigan (0.21 km^2), both underlain by continuous permafrost without any glacial input. Unlike the Upper Kuparuk watershed, which is more vegetated, Cape Bounty has minimal vegetation and even lower amounts of precipitation: only roughly 160 mm of precipitation falls each year, mostly in the form of snow (Mekis and Hogg, 1999). The mean rainfall recorded at the Cape Bounty meteorological station between June and August for 2003–2023 was 45.4±24.5 mm, with a minimum of 15.2 mm in 2014 and a maximum of 124.4 mm in 2019.

Although the neighboring Cape Bounty headwater catchments likely experience very similar meteorological and geologic controls, they do exhibit some important differences. Ptarmigan has two active layer detachments (ALDs). The ALDs cover 10.8 % of the surface area of Ptarmigan. The ALDs initiated in 2007 and the headwall retrogressively retreated over the next four years by a total of $\sim 45 \pm 5$ m, stabilizing at the end of the 2011 summer season (Beel et al., 2020). Although the retrogressive growth of these features may classify them as retrogressive thaw slumps in some literature, we follow the terminology used in previous Cape Bounty literature and refer to them as ALDs, distinguishing between periods of active growth ("active") and quiescence ("stable"). We compare the runoff responses of the Ptarmigan and Goose catchments during periods when ALDs are active versus stable, under the simplifying assumption that meteorological differences between the time periods exert a similar influence on both catchments.

At the Cape Bounty sites, the WestMet meteorological station provides hourly local temperature and rainfall data (Beel et al., 2018) at a hilltop north of the catchments (Fig. 1b). Discharge data were collected at gaging stations located at the outlets of the catchments, consisting of rectangular weirs (2006–2008) and 20 cm (8″) cutthroat flumes (2009–2017). They were equipped with Onset U20 (2006–2014) and vented Stevens SDX (2016–2017) pressure transducers to measure water level at 10 min intervals (Beel et al., 2020). Additionally, water samples were collected daily at each outlet, and analyzed for: (1) dissolved organic carbon (DOC) using a Shimadzu TOC-VPCH/TNM system (Fouché et al., 2017); (2) total dissolved solids (TDS), or major ion concentration, using ion chromatography, with individual cation and anion concentrations summed to derive TDS (Beel et al., 2020); (3) suspended sediment (SS), where samples were filtered through pre-weighed GF/F filters, which were then dried and reweighed to measure sediment mass per volume (Beel et al., 2020); and (4) particulate organic carbon (POC) by combusting the SS filters in a CHN elemental analyzer (Beel et al., 2020). We assess how material fluxes respond to precipitation in the two headwater catchments, with a focus on times when the ALDs are active.

3 Methods

We estimate how precipitation intensity and ambient conditions (including antecedent moisture, seasonal development of the active layer, and erosion of near-surface soils) affect streamflow and material flux response to precipitation using ensemble rainfall-runoff analysis (ERRA; Kirchner, 2024), a recently developed technique derived from general methods for estimating impulse responses in nonlinear, nonstationary, and heterogeneous systems (ERRA; Kirchner, 2022). ERRA uses multiple linear regression of precipitation and streamflow time series to estimate the ensemble-average response of streamflow to precipitation at the whole-catchment scale. Here, for the first time, we are also applying the approach to quantify material flux responses to precipitation.

For a given precipitation and streamflow/material flux time series, the simplest form of this linear regression is:

$$Q_i = \sum_{k=0}^{m} \beta_k P_{i-k} + c + \sigma_i, \quad (1)$$

where Q_i is streamflow or material flux, both defined as "runoff" when normalized by catchment area, at the ith time step, P_{i-k} is precipitation falling k time steps earlier for a total of m time steps, β_k is the impulse response function at lag k, c is the regression constant, and σ_i is the residual error associated with the runoff at hour i.

Conventional linear regression analysis assumes that the residual errors are temporally independent (white noise), but typical environmental time series are characterized by autocorrelated noise. Time series runoff data can exhibit autocorrelated residuals because catchments integrate inputs over characteristic response times that can be longer than the sampling interval. As a result, successive observations are not statistically independent; streamflows (and other fluxes) at a given time partly reflect earlier precipitation and storage conditions. This temporal persistence leads to autocorrelated noise, which can bias uncertainty estimates and overstate statistical significance without necessarily affecting the estimated mean response itself (Kirchner, 2024). This is further explained in Sect. 2 of Kirchner (2022) and motivates ERRA as an approach for estimating the original runoff response coefficients β_k using the recursion relationship (Eq. 22 of Kirchner, 2022).

The coefficients β_k across a range of lags k comprise the Runoff Response Distribution (RRD), which estimates the ensemble average runoff response to a unit pulse of rainfall. The uncertainties in these coefficients will depend on the number of coefficients that need to be estimated from a given volume of data. We resolve the signal in the RRD while minimizing uncertainty by aggregating the time steps and averaging over different intervals to limit the number of coefficients that must be estimated.

To apply this approach at the Upper Kuparuk and Cape Bounty catchments, we assume that measured precipitation is rainfall if the temperature at the mean basin elevation is above 0 °C. At the dry adiabatic lapse rate of 9.8 °C km^{-1}, this corresponds to temperatures above 2 °C at the Upper Kuparuk (where the weather station is located at the outlet, 200 m below the mean elevation), and above −0.5 °C at Goose and Ptarmigan (where the weather station is located about 50 m above the mean basin elevation) (Fig. 1). Our analysis focuses on summer rainfall events, rather than annual snowmelt or the occasional summer snowstorms. While snowmelt can dominate the annual peak discharge in these catchments, rainfall is the primary driver of streamflow variability and event-scale peak flows during the summer season following snowmelt.

The summertime hydrometeorological observations at Upper Kuparuk are mostly complete (data availability is > 90 % for any given year; Fig. S1a), facilitating analyses of how meteorological forcing and subsurface changes affect runoff. By contrast, data availability is ∼ 50 % for any given year at the Cape Bounty catchments (Fig. S1b–c), where we investigate how active layer detachments (ALDs) affect runoff response to rainfall.

At Upper Kuparuk, we test how the runoff response distribution changes with hourly rainfall intensity and antecedent streamflow, each year and each summer month (June, July, and August). We also test how the RRD varies with 12 candidate predictor variables: (1) total summer precipitation for the current and (2) previous summer; (3) total summer rainfall for the current summer; the (4) current and (5) previous summers' average rainfall intensities; (6) maximum snow depth and (7) total snowfall since the previous summer; (8) average temperatures during the preceding winter and spring; (9) average summer temperature; (10) cumulative degree days above 0 °C for the current summer, (11) maximum spring streamflow, and (12) the current summer's thaw rate. Because different fractions of data may be missing in individual years (Fig. S1a), we calculate total summer precipitation and rainfall as the average of the available data, multiplied by the combined duration of the three summer months. These seasonal precipitation and rainfall totals are used as approximate, contextual descriptors to facilitate interannual comparison and do not enter directly into the RRD calculations, which are based on observed event-scale rainfall–runoff pairs. Winter and spring temperatures are calculated as averages from 1 November to 31 May. The maximum pre-summer flood discharge is determined by identifying the highest runoff value in the daily time series from 1 April to 31 May. The annual rate of subsurface thaw is calculated based on daily ground temperature data at 5 cm intervals down to 60 cm depth between 1994 and 2010. For each day, we set the thaw depth to be the deepest layer that is at or above 0 °C. The snow depth and subsurface thaw rate data overlap with our precipitation and runoff records at Upper Kuparuk for only 5 years, precluding their use as long-term explanatory variables, but they provide supplementary information to help interpret the results. These variables are treated as

candidate, physically motivated descriptors rather than independent predictors; collinearity among them is expected given the coupled nature of precipitation, temperature, and thaw processes in permafrost catchments, and they are used to aid interpretation rather than to construct a parsimonious predictive model.

We evaluate each of the candidate predictors individually, and also assess pairwise combinations of the 12 candidate predictors using two-variable multiple linear regressions. For each possible predictor pair, a linear model relates predictors to peak runoff response and the resulting coefficient of determination (R^2) quantifies their joint explanatory power.

The added variable plots (Cook and Weisberg, 1982) show the individual contribution of each predictor to the peak runoff response to rainfall. These plots illustrate the partial relationship between each predictor and the response variable, after accounting for the influence of the other predictors in the model.

Runoff data obtained from Arp et al. (2017), precipitation data from Kane et al. (2021), snow depth data from Kane et al. (2021), and subsurface thaw data from Kane et al. (2021, updated) support the Upper Kuparuk analyses (Fig. S2).

One motivation for examining rainfall-driven runoff responses is to better quantify event-scale mobilization of carbon and other materials from permafrost landscapes. Since the ERRA approach can be applied to quantify the coupling between any interrelated time series, ERRA can also quantify daily material fluxes at the Cape Bounty catchments. Instead of quantifying the overall annual increase in material concentrations in streams, as in Beel et al. (2020), the ERRA approach quantifies how much stream DOC, TDS, SS, and POC fluxes increase in response to rainfall, and how long these increases last. Given that the material flux data are only available for 92 individual days, we set the maximum response time to be 5 continuous days ($m = 5$ d in Eq. 1) to avoid overfitting and to maximize the sample size.

4 Results and Discussion

Our analysis first examines how runoff responds to short-term meteorological conditions, annual meteorological conditions, and increasing active layer thickness at Upper Kuparuk, given its longer and more complete record. We then investigate how ALDs affect rainfall-runoff behavior by comparing the Goose and Ptarmigan catchments when ALDs are active and stable. Finally, we quantify the material flux runoff response to rainfall at Goose and Ptarmigan.

As catchment size increases, ERRA increasingly reflects the spatial integration of multiple flow pathways, soil depths, and contributing areas, each with potentially different rainfall thresholds, storage capacities, and timing of response. Consequently, RRD curves for larger catchments are expected to be smoother and delayed in response, whereas RRD curves for smaller catchments are expected to be more sensitive to event-scale variability.

4.1 Peak runoff response is sensitive to antecedent effective wetness

We initially examine runoff response to rainfall at Upper Kuparuk by considering the entire 14-year record of hourly data, aggregated into 10 h time steps (Fig. 2a). The runoff response distribution (Fig. 2a; where the lag time is k and RRD is β in Eq. 1) peaks approximately 20 h after rain falls ($k = 2$ in Eq. 1) and decays toward zero over the following 300 h ($m = 30$ in Eq. 1), with a runoff coefficient over this 300 h period (the area under the RRD curve) of 57 %. Conditioned on rainfall events, $\sim$ 57 % of 10 h rainfall input is exported as runoff within $\sim$ 12 d. Although derived at event-scale, this rainfall-conditioned runoff coefficient is consistent with previous water-balance studies at Upper Kuparuk, which report that approximately 60 %–70 % of annual precipitation is exported as runoff due to limited subsurface storage in continuous permafrost terrain (McNamara et al., 1998; Déry et al., 2004; Youcha and Stuefer, 2026). The peak of the runoff response distribution corresponds to 0.6 % of the hourly rainfall rate (or an equivalent of 0.6 % of the hourly rainfall discharges at the 20th h), consistent with the duration of the runoff response.

Comparing runoff response distributions across different ranges of 10 h lagged streamflow shows how antecedent hydraulic conditions affect runoff response to precipitation (Fig. 2b). Figure 2b shows that higher levels of antecedent streamflow yield a sharper and stronger peak runoff response, with these effects becoming asymptotic at relatively high antecedent streamflow levels (Fig. 2c). It corresponds to discharge values of 4.4 $m^3 s^{-1}$ for Upper Kuparuk, which is above the median discharge value (3.13 $m^3 s^{-1}$).

The five-fold increase in peak RRD with antecedent runoff is consistent with findings from other permafrost catchments and cold-region catchments, where antecedent streamflow reflects the degree of hydrologic connectivity and effective storage within the active layer. Numerous studies have shown that higher antecedent streamflows are associated with enhanced rainfall responsiveness (e.g., Dingman, 1971; Quinton and Marsh, 1999; Xiao et al., 2022; Massari et al., 2023; Knapp et al., 2025).

In Fig. 2c, the peak runoff response appears to plateau beyond a certain antecedent streamflow threshold. We speculate that this behavior may reflect increasing subsurface saturation and routing of runoff as near-surface flow, consistent with observations at a smaller scale within the catchment (Rushlow and Godsey, 2017). One potential geomorphic expression of this process in permafrost landscapes is water tracks, which are narrow, linear features that concentrate surface or near-surface flow in permafrost landscapes (Evans et al., 2020; Del Vecchio and Evans, 2025). This asymptote may represent the antecedent streamflow at which water tracks be-

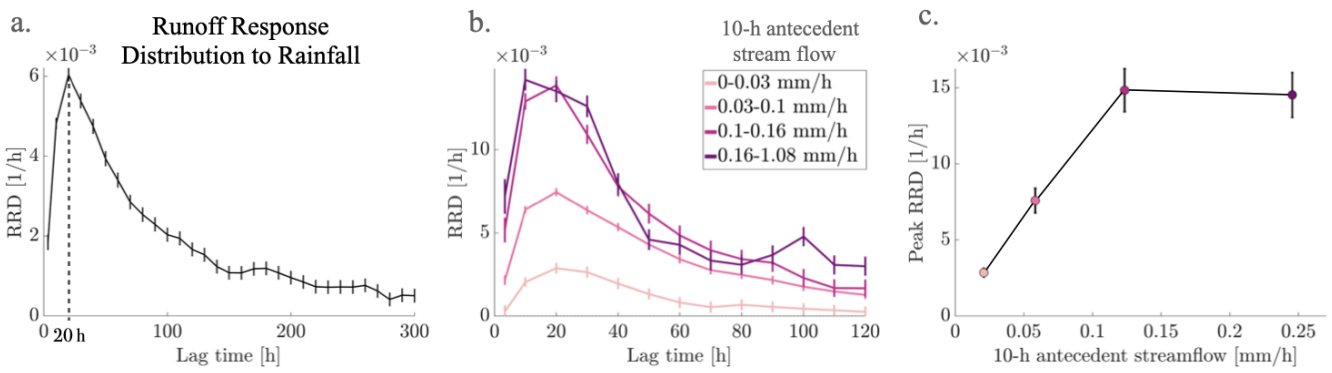


Figure 2. Runoff sensitivity to antecedent streamflow at Upper Kuparuk. **(a)** Average runoff response per unit rainfall at Upper Kuparuk (runoff response distribution using all available data, aggregated to 10 h time steps); **(b)** Runoff response distributions for different ranges of antecedent streamflow for different ranges of 10 h antecedent streamflow. We selected percentile thresholds (37.5th, 75th, and 87.5th percentiles) to provide greater resolution at high antecedent streamflow while retaining sufficient observations within each range to resolve the runoff response distribution; **(c)** Peak height of runoff response distributions in **(b)**, as a function of 10 h antecedent streamflow. Peak runoff response increases approximately linearly with antecedent streamflow, up to an apparent asymptote. Error bars indicate one standard error.

come hydrologically connected to stream channels, enabling rapid routing of rainfall to the stream with limited additional storage attenuation, consistent with modeling results within the basin (Stieglitz et al., 2003). Thus, we suggest that antecedent streamflow may be a proxy for antecedent effective wetness, where lagged streamflow is an operational proxy for the hydrologic state of the drainage network, reflecting near-surface wetness, connectivity, and drainage efficiency rather than the absolute storage.

4.2 Peak runoff response increases linearly with precipitation intensity

To assess how runoff response varies with rainfall intensity, we use the nonlinear response function (NRF; Kirchner, 2024), which equals the runoff response distribution for a given range of rainfall rates, multiplied by the time step and the rate of precipitation (Fig. 3a). The NRF measures the increase in streamflow resulting from one time step of precipitation at a given intensity. Whereas the RRD is a measure of runoff response per unit rainfall, the NRF is a measure of total runoff response per time interval of precipitation (falling at a given rate), and thus more clearly reveals how runoff response varies with precipitation intensity. As shown in Fig. 3b, higher rainfall intensities generate larger runoff responses as measured by the NRF. The peak height of the NRF increases approximately linearly with precipitation intensity.

Figure 3c shows how peak runoff response varies jointly as a function of precipitation intensity and antecedent streamflow (indicated by the different curves, each corresponding to a different range of 10 h antecedent streamflow). For each range of antecedent streamflows (i.e., for each curve), peak runoff response is a weakly nonlinear function of rainfall rate.

4.3 Stronger runoff response during wet summers, and following cold winters and springs

Weather conditions vary from year to year at Upper Kuparuk, and their effects on runoff behavior can be illustrated by comparing runoff response distributions among individual years. The runoff response distributions for different years vary considerably, with some years exhibiting strong responses and others displaying weak responses (Fig. 4). For example, the peak runoff response distribution for 2009 corresponds to 1.3 % of the hourly rainfall rate, whereas peak runoff responses in 2005 and 2011 correspond to less than 0.3 % of the hourly rainfall rate (Fig. 4).

To evaluate the potential mechanisms behind this variability, we examine how year-to-year variations in runoff response reflect differences in both precipitation and temperature conditions, particularly those that influence subsurface storage capacity with the 12 potential explanatory variables outlined in the Methods section. The Methods section details the measurement of each variable. Figure S3 compares each explanatory variable individually with peak runoff response to rainfall. Recall that because maximum snow depth and thaw rate data are only available for 5 rather than 12 full years, these two explanatory variables only supplement our discussion.

Total current summer precipitation and rainfall (Fig. S3a–b) are first-order controls on peak runoff response to rainfall. Ignoring this first-order control, the pair of predictor variables with the highest R^2 value in our multiple linear regression analyses is total summer precipitation and average temperatures during the preceding winter and spring. Figure 5a shows the model fit for this best-performing pair. To facilitate interpretation and compare the relative influence of each variable, we standardized both predictors as z-scores and re-

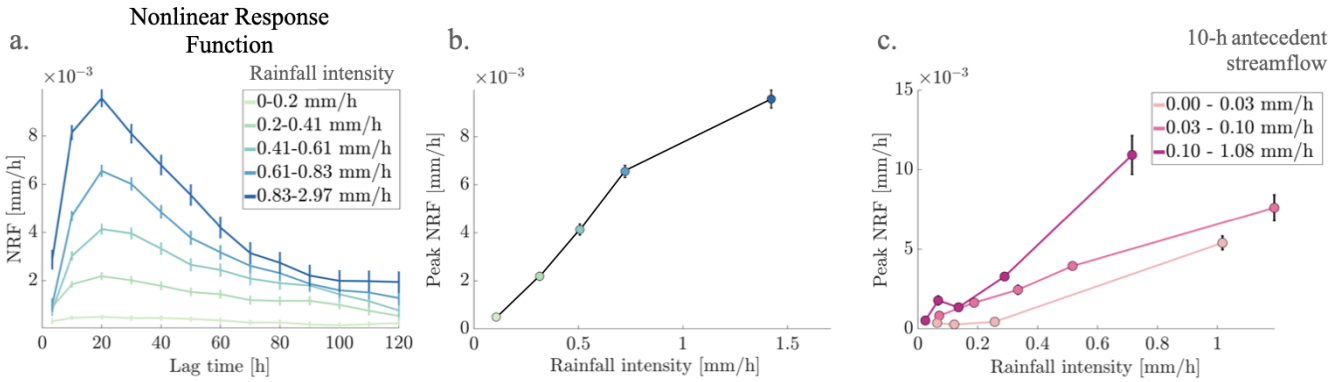


Figure 3. Runoff response at Upper Kuparuk increases linearly with rainfall intensity. **(a)** Nonlinear response functions depicting how runoff response varies with precipitation intensity, evaluated at evenly spaced precipitation intensities from 4 to 40 mm d^{-1}; **(b)** Peak height of nonlinear response functions in **(a)** increases roughly linearly as a function of precipitation intensity; **(c)** Peak height of nonlinear response functions for different ranges of antecedent streamflow (indicated by the differently colored curves) and precipitation intensity. Higher antecedent streamflow makes runoff more sensitive to precipitation intensity. All results obtained by aggregating hourly Upper Kuparuk time series to 10 h intervals. Error bars indicate one standard error.

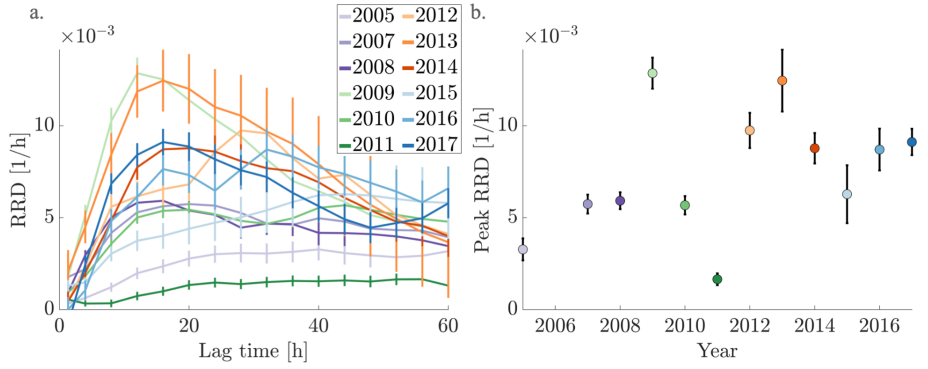


Figure 4. Year-to-year variability in runoff response distributions at Upper Kuparuk shows a sixfold range, with no clear temporal trend. **(a)** Runoff response distributions for each year; **(b)** Peak height of the distributions in **(a)** and their associated error bars plotted as a function of year. Each year is shown in a distinct color, used consistently throughout the manuscript. All results obtained by aggregating hourly Upper Kuparuk time series to 4 h intervals. Error bars indicate one standard error.

port the regression equation as:

$$z_\beta = (0.66 \pm 0.23) z_{\mathrm{Ps}} - (0.46 \pm 0.23) z_{\mathrm{Tw}} + c, \quad (2)$$

where z_β is the z-score–transformed peak runoff response to rainfall, z_{Ps} is the z-score–transformed total summer precipitation, z_{Tw} is the z-score–transformed average temperatures during the preceding winter and spring, and c is a baseline constant.

The added variable plots (Fig. 5b–c) show that the regression model performs fairly well ($R^2 = 0.58$), and critically, it shows that both predictors are statistically significant: peak runoff response is influenced by both total summer precipitation ($p = 0.01$) and average temperatures during the preceding winter and spring ($p = 0.03$).

The correlation with summer precipitation is consistent with the patterns observed in Figs. 2 and 3, where peak runoff response shows a strong positive relationship with antecedent streamflow and rainfall intensity. In addition to average summer precipitation, average temperatures during the preceding winter and spring seasons show a weaker signal, negatively correlated with runoff response (Fig. 5). Winter–spring temperature may reflect several antecedent processes, including snowpack evolution, snowmelt timing, and near-surface freeze–thaw conditions, that could influence hydrologic conditions entering the summer season (Jan and Painter, 2020). However, spring hydrologic conditions integrate these and other interacting processes, and our analysis cannot identify the mechanism underlying this correlation. The relationship nevertheless suggests that conditions preceding the summer rainfall season may contribute to interannual variability in runoff response.

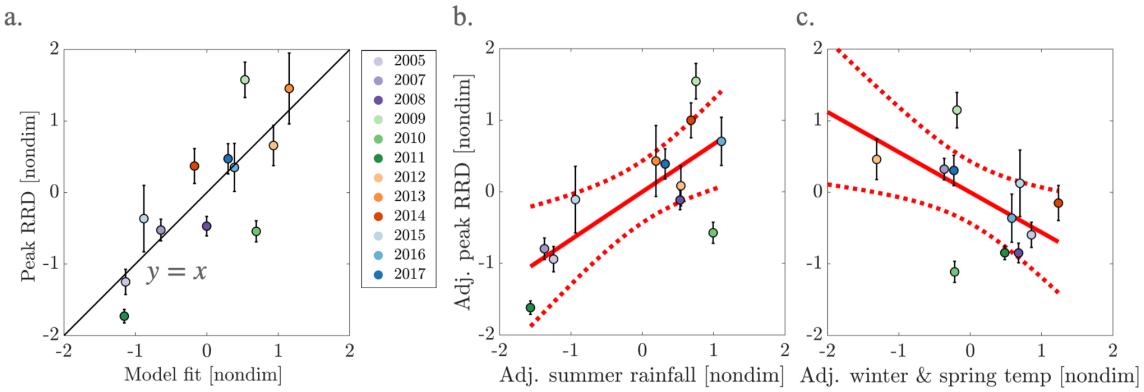


Figure 5. Factors influencing annual peak runoff response to rainfall at Upper Kuparuk. All variables shown as z-scores. **(a)** Peak of the runoff response distribution for each summer, compared to fitted values of a linear model with total summer rainfall and average temperatures during the preceding winter and spring as explanatory variables. The diagonal line indicates a 1 : 1 relationship. **(b)** Added variable plot (i.e., leverage plot) showing relationship between RRD peak height and total summer rainfall, corrected for linear effects of winter and spring temperatures. **(c)** Added variable plot showing relationship between RRD peak height and winter and spring temperatures, corrected for linear effects of total summer rainfall. Error bars indicate one standard error.

4.4 Runoff is more sensitive to rainfall earlier in the summer

Previous studies across Alaskan permafrost catchments have demonstrated that progressive active layer deepening alters runoff generation by increasing subsurface storage and modifying vertical profiles of hydraulic conductivity, commonly leading to reduced rainfall responsiveness later in the summer (Hinzman et al., 1991; McNamara et al., 1997; Kane et al., 2000; Stieglitz et al., 2003; Jorgenson et al., 2025). ERRA provides a diagnostic framework to quantify the magnitude of this seasonal effect at event scales. Specifically, we examine how peak runoff response to rainfall varies across summer months, providing a quantitative assessment of how progressive thaw modulates runoff response over the course of the season. Peak runoff response declines by approximately 25 % in peak runoff response from June to August (Fig. 6).

As shown in Sect. 4.1, antecedent streamflow can increase peak runoff response by nearly a factor of five. To disentangle this effect from that of monthly variations, Fig. S4 shows how the antecedent streamflow response varies by month. The monthly decline in runoff response is small compared to the variation driven by antecedent streamflow, revealing possible seasonal controls on runoff response. Relative to prior studies that document strong seasonal shifts in runoff generation with active layer development, the magnitude of the seasonal effect observed here is modest, indicating that thaw-related increases in storage modulate, but do not dominate, peak event-scale runoff response in the Upper Kuparuk.

To evaluate what drives this decline, we assess monthly changes in meteorological conditions in Fig. S5. This diagnostic step is intended to rule out alternative atmospheric explanations before attributing the seasonal decline in runoff response to thaw-related changes in subsurface storage and

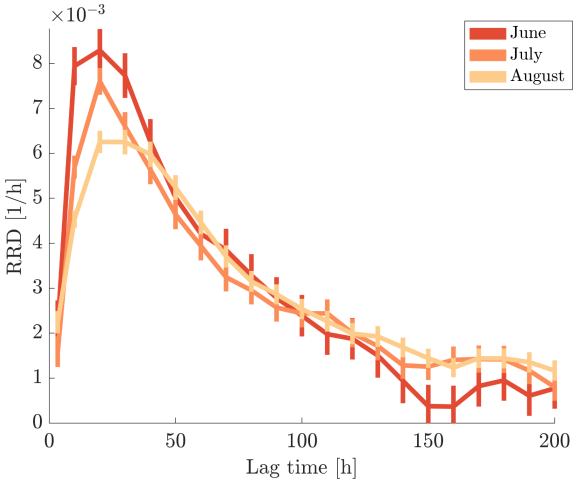


Figure 6. The Peak Runoff Response Distribution decreases by 25 % between June and August at Upper Kuparuk. We show the runoff response distribution for June (red), July (orange) and August (yellow). All results obtained by aggregating hourly Upper Kuparuk time series to 10 hour intervals. Error bars indicate one standard error.

flow pathways. Precipitation totals, air temperature, and rainfall intensity do not show consistent trends across the summer months, suggesting that changes in atmospheric forcing are unlikely to explain the decrease in peak runoff response. Similarly, seasonal variations in evaporation and transpiration do not align with the decline in runoff response: transpiration typically peaks in July and declines thereafter (Déry et al., 2005; Liljedahl et al., 2011; Helbig et al., 2020), but the peak runoff response declines monotonically from June to August.

By contrast, active layer thaw depth increases substantially from June to August, expanding from approximately 20 to 50 cm on average at the Upper Kuparuk catchment (Shiklomanov, 2014). This seasonal deepening of the active layer, and the associated increase in subsurface storage capacity and depth-dependent hydraulic conductivity, has been widely shown to reduce rainfall responsiveness in permafrost catchments by promoting infiltration and delayed subsurface flow (e.g., Stieglitz et al., 2003). As a result, peak runoff response decreases. These findings support the hypothesis that seasonal expansion of subsurface storage capacity through thawing can decrease runoff response (e.g., McNamara et al., 1997, 1998; Stieglitz et al., 2003). This agrees with previous studies in the Upper Kuparuk where sequential storms through a summer had increasing old water contributions (McNamara et al., 1997), and lower runoff ratios (Q/P) (McNamara et al., 1998), as well as more recent work documenting enhanced subsurface storage, delayed flow pathways, and reduced rainfall responsiveness later in the summer in permafrost catchments (Stieglitz et al., 2003; Liljedahl et al., 2011). Our results are consistent with these findings, but indicate that, even after accounting for event-to-event variability in rainfall magnitude, intensity, and structure, the seasonal influence of thaw depth on peak runoff response is smaller than the variability driven by other factors like antecedent streamflow (Fig. 2b–c). Similar conclusions were reached by Jorgenson et al. (2025), who showed using environmental tracers that permafrost thaw deepens subsurface flowpaths, but that the hydrologic effects of thaw can be obscured by simultaneous changes in precipitation regime.

In other permafrost catchments, thawed-layer storage capacity may play a more prominent role in regulating runoff response, depending on soil properties and flowpath structure. Numerous studies have documented that hydraulic conductivity in permafrost terrain varies by orders of magnitude both vertically within the active layer and laterally across hillslopes, reflecting differences in soil texture, ice content, organic horizons, and soil structure (Hinzman et al., 1991; Stieglitz et al., 2003; Genxu et al., 2017; Neilson et al., 2018; O'Connor et al., 2020; Sjöberg et al., 2021; Hamm and Frampton, 2021). These contrasts exert strong controls on infiltration capacity, subsurface storage, and the partitioning between rapid surface runoff and delayed subsurface flow. Vegetation is relevant in this context insofar as it co-varies with soil development and organic layer thickness, which influence near-surface hydraulic conductivity and water retention, rather than acting as an independent control on runoff response. As a result, the importance of thawed-layer storage in regulating runoff varies across permafrost landscapes and depends on the combined effects of soil texture, active layer structure, and anisotropy in hydraulic conductivity, rather than on thaw depth alone.

In addition to vertical storage effects, runoff generation in permafrost catchments is strongly influenced by threshold-controlled lateral hydrologic connectivity. As soil moisture increases and the active layer deepens, previously disconnected portions of the near-surface soil profile can become hydraulically connected to downslope flow pathways and the channel network, producing nonlinear increases in runoff response (Quinton and Marsh, 1999; Quinton et al., 2000). This behavior is characteristic of permafrost environments, where low permeability at depth constrains flow to shallow horizons and promotes rapid lateral transmission once saturation thresholds are exceeded. In this context, antecedent effective wetness reflects not only the availability of subsurface storage, but also the degree to which laterally connected flow paths are activated at the time rainfall occurs. Such threshold behavior provides a physical basis for the strong sensitivity of peak runoff response to antecedent hydrologic state observed in Fig. 2b–c, and may explain why antecedent streamflow exerts a larger control than gradual seasonal increases in thaw depth.

4.5 Stronger runoff response to rainfall in years when active layer detachments are actively growing

Active layer detachments (ALDs) at Cape Bounty provide a natural experiment to examine how erosion could alter runoff response to rainfall in Arctic catchments, complementing the analysis of gradual seasonal and interannual controls on runoff response to rainfall. Lamoureux and Lafrenière (2009) documented increased discharge, enhanced hydrologic connectivity among ALDs, and flow impoundment associated with extensive ALD activity at Cape Bounty, while Lamoureux et al. (2014) noted persistent heterogeneity in runoff following disturbance. More recent work has shown that permafrost disturbances, including ALDs, strongly influence dissolved and particulate fluvial fluxes and catchment-scale hydrologic behavior (e.g., Beel et al., 2018, 2020). Similarly, other mass movement events such as retrogressive thaw slumps are known to impact catchment hydrology (e.g., Connon et al., 2014; Lafrenière and Lamoureux, 2019; Kokelj et al., 2021), but it has been difficult to quantify these effects at the event-scale and to assess whether hydrologic responses recover following stabilization. ERRA enables a complementary event-scale characterization by quantifying how hourly rainfall inputs modify runoff response during periods of ALD activity versus quiescent conditions, and relative to an undisturbed reference catchment. We analyze long-term data from the Cape Bounty region, which includes two neighboring catchments of comparable size and climate (Ptarmigan and Goose). Two active layer detachments (ALDs) that initiated in 2007 disturbed roughly 10.8 % of the Ptarmigan catchment, stripping the upper unfrozen material along the main channel (Fig. 1b). The headwalls of the ALDs continued to erode through 2011, whereas the neighbouring Goose catchment remained geomorphically stable (Beel et al., 2021).

Figure 7 compares the runoff response to rainfall for both catchments, separating time periods with and without ALD

activity. To isolate the effect of ALDs from meteorological variability, we compare runoff response at Ptarmigan before and after ALD activity, and contrast it with runoff response at Goose over the same time periods.

The results show that, on average, peak runoff response at Ptarmigan is four times higher during the five years with ALD activity (2007–2011) than during the 10-year post-ALD period (2012–2021). In contrast, the neighboring Goose catchment shows no substantive difference in runoff response between the two time periods, suggesting that the changes in runoff response at Ptarmigan cannot be attributed to meteorological differences between the two periods. Moreover, the peak runoff response at Goose is about three times lower than at Ptarmigan during ALD-active years, reinforcing the inference that the changes at Ptarmigan are due to geomorphic disturbance rather than climate variability.

Although we lack pre-ALD data for Ptarmigan, the sharp decline in runoff response after stabilization suggests a strong effect of ALDs on runoff response. One plausible mechanism is that ALDs erode near-surface soil layers, exposing ice-rich permafrost (up to 80 % ice by volume) with very low permeability (e.g., Paquette et al., 2020). This scar area may retain a shallower active layer for several years, reducing infiltration and enhancing surface runoff. Thus, although the ALD areas are only increasing by a few 10s of square meters each active year, the large scar area can still have a significant impact on the runoff response.

After ALD stabilization, runoff response at Ptarmigan declines to roughly match the runoff response at Goose. One plausible explanation is that the hypothetical ice-rich layer at the sliding interface progressively thaws and drains, increasing subsurface storage capacity over time, reducing the efficiency with which rainfall is converted to runoff. Although vegetation cover at Ptarmigan remains minimal during the study period (Fig. 1c), even limited organic layer development may influence near-surface hydrologic behavior. Disentangling the relative roles of thaw depth evolution, subsurface drainage, and surface recovery would require targeted measurements of active layer thickness, soil moisture, and surface properties within scar zones, which are beyond the scope of the present dataset.

Although the spatial extent of ALDs is limited to merely 10 % of the catchment, the results demonstrate that ALD activity substantially increases the flashiness of runoff response to rainfall, as quantified by ERRA through amplified peak response. This enhanced flashiness does not imply basin-scale flooding, but it does indicate a greater sensitivity of affected headwater catchments to rainfall inputs, with potential consequences for localized drainage exceedance, erosion, and infrastructure performance at small spatial scales (e.g., Van der Sluijs et al., 2018; Ackerson et al., 2021; Luo et al., 2022).

4.6 Catchments with ALDs act as sources of biogeochemical and sediment export during rainfall

Alongside rainfall/runoff data, Cape Bounty has multiple years of DOC, TDS, SS and particulate organic carbon (POC) concentration data collected in streamflow at approximately daily intervals (Beel et al., 2020). These concentration measurements enable a detailed event-scale analysis of how material fluxes in streamflow respond to rainfall at Cape Bounty. ERRA provides a way to quantify the timing, magnitude, and persistence of material fluxes to rainfall.

Here, we define material fluxes as concentrations times streamflow normalized by catchment area. Figure S6 shows the time series of material fluxes alongside rainfall and runoff time series data. As shown in Beel et al. (2020), annual DOC fluxes are consistently higher at Goose than Ptarmigan, despite transient DOC enrichment during ALD activity. TDS fluxes are persistently higher at Ptarmigan and rise further while the slides are active. SS and POC fluxes at Ptarmigan increase by an order of magnitude during ALD activity, whereas both fluxes remain minimal at Goose throughout the record. Figure S7 shows how material fluxes are correlated with precipitation and discharge. Material fluxes show no clear correlation with precipitation. By contrast, discharge is positively correlated with material fluxes, particularly for TDS, SS, and POC at Ptarmigan; note that because discharge is part of the material flux calculation, positive correlations are expected (unless concentrations decrease more-than-proportionally with increasing discharge). TDS, SS, and POC fluxes increase more steeply as a function of discharge at Ptarmigan than at Goose; by contrast, DOC response to increasing discharge is broadly similar between the two catchments.

Although there does not appear to be a correlation between material fluxes and precipitation, there can still be a relationship that is not well captured in a simple correlation analysis. Rainfall influences material export in Arctic catchments through both mobilization and dilution processes, and the resulting concentration–discharge relationships can exhibit strong hysteresis or near-chemostatic behavior depending on solute availability and flow-path activation (e.g., McNamara et al., 1998; Frey and McClelland, 2009; Shogren et al., 2019, 2022, 2024). Event-scale studies have shown that rainfall can generate short-lived but disproportionate contributions to suspended sediment, particulate organic carbon, and solute fluxes (Lamoureux and Lafrenière, 2014; Beel et al., 2018; Xiao et al., 2022) transported along shallow and near-stream flow paths (e.g., Bowden et al., 2008; Tank et al., 2016), while dissolved constituents such as DOC may remain elevated for days following rainfall (Koch et al., 2021). Collectively, this work demonstrates that rainfall exerts strong control on material export, but the timing (e.g., lag) and persistence of event-scale flux responses remain incompletely constrained. Here, we extend ERRA beyond runoff to quan-

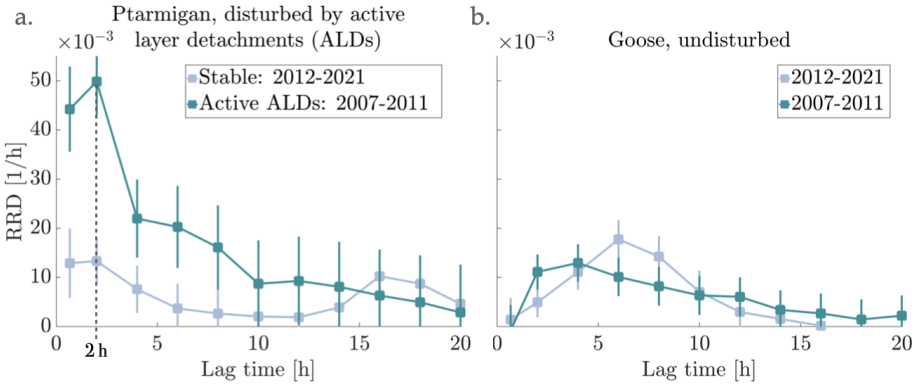


Figure 7. Runoff response distributions for Ptarmigan **(a)** and Goose **(b)**. **(a)** At Ptarmigan, active layer detachments disturbed ∼ 10 % of the catchment between 2007 and 2011. Runoff at Ptarmigan was more responsive to rainfall during this period (green) than during the following 10 years (2012–2021, blue). **(b)** At the adjacent Goose catchment, where no active layer detachments were observed, runoff responses to rainfall were similar during both periods. All results obtained by aggregating hourly Ptarmigan and Goose time series to 2 h intervals. Error bars indicate one standard error.

tify the event-scale material flux response to rainfall, allowing direct comparisons of the timing, magnitude, and persistence of DOC, TDS, SS, and POC export following rainfall, independent of background seasonal trends or cumulative fluxes at Ptarmigan and Goose.

In this analysis, we substitute runoff in Eqs. (1)–(2) with material fluxes (concentration multiplied by runoff), while retaining precipitation (P) as the driver. Figure 8 illustrates how runoff fluxes of DOC, TDS, SS, and POC respond to rainfall at Ptarmigan and Goose. Figure 8 shows that both catchments exhibit notable DOC and TDS flux runoff responses that peak within 1 d of rainfall and decline over the subsequent 2 d. Figure 8e and f show the daily water flux runoff response distribution to rainfall, which produces a similar rapid response that declines over the course of 2 d as the DOC and TDS flux runoff response. These results, together with the previous findings of Beel et al. (2020), support the conclusion that rainfall mobilizes DOC and TDS at these catchments. If rainfall intensity and frequency increase as projected under climate change (Bieniek et al., 2022; Bintanja et al., 2020), stream DOC and TDS concentrations may increase (and thus stream DOC and TDS fluxes may increase more than proportionally to increases in discharge; Tank et al., 2023).

Beel et al. (2020) compared annual fluxes at Ptarmigan and Goose and showed that the annual DOC flux is consistently higher at Goose, despite transient DOC enrichment during ALD activity at Ptarmigan. ERRA reveals that, at event scales, DOC flux responses to rainfall are similar between the two catchments (Fig. 8a). Therefore, the higher annual DOC flux observed at Goose cannot be explained by greater rainfall responsiveness and must instead reflect differences in DOC sources, production, or availability. By contrast, the annual major ion (TDS) flux increased after the 2007 ALDs at Ptarmigan and remained high during the following years, a pattern that is absent at Goose (Beel et al., 2020). Figure 8b also shows that the event-scale response of TDS runoff fluxes to rainfall is four times higher at Ptarmigan than at Goose, suggesting that the ALDs increased the TDS runoff response to rainfall.

According to Beel et al. (2020), annual Ptarmigan SS and POC fluxes increased 15–30 fold in the first season following ALD initiation and remained approximately an order of magnitude above background levels during the five years of active erosion, a pattern absent at Goose. Furthermore, catchments affected by ALDs at Cape Bounty exhibited POC-dominated stream carbon fluxes for more than five years after the initial disturbance (Beel et al., 2021). Figure 8c–d show substantially stronger SS and POC flux responses to rainfall at Ptarmigan than at Goose, indicating that rainfall events more readily mobilize sediment and particulate carbon at the disturbed catchment. Together, these observations suggest that ALDs may not only increase cumulative material export, but may also enhance the sensitivity of TDS, SS, and POC export to rainfall for several years following disturbance. Given projected increases in Arctic rainfall intensity and frequency, as well as the growing prevalence of ALDs across Arctic landscapes, downstream aquatic systems could experience increasingly frequent episodes of elevated TDS, SS, and POC fluxes (Tank et al., 2023).

5 Summary and implications for catchment behavior in a warming climate

Conceptual models describing runoff generation in permafrost landscapes have a long history and consistently emphasize the role of active layer development, subsurface storage, and threshold-controlled hydrologic connectivity in shaping streamflow and material export (Quinton and Marsh, 1999; Quinton et al., 2000, 2009; Quinton and Carey,

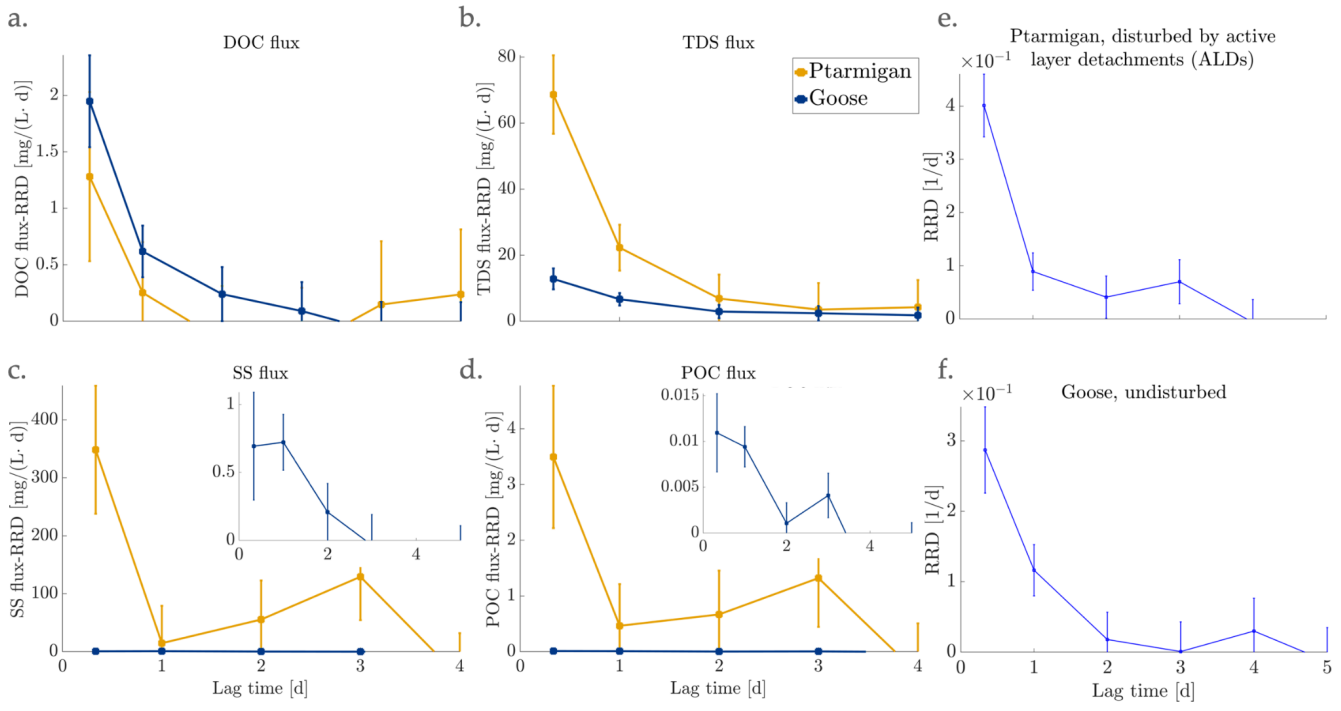


Figure 8. DOC, TDS, SSC, and POC runoff response distributions are comparable to water flux runoff response distribution to rainfall. **(a–d)** Runoff response distributions quantifying how rainfall inputs increase runoff fluxes of dissolved organic carbon (DOC, **a**), total dissolved solids (TDS, **b**), suspended sediment (SS, **c**), and particulate organic carbon (POC) as inferred from suspended sediment concentrations **(d)**. Subpanels in **(c)** and **(d)** zoom into the Goose SS flux-RRD and POC flux-RRD, respectively. Ptarmigan and Goose catchments are shown by orange and blue lines, respectively. **(e–f)** Panels **(e)** and **(f)** compare these responses to water flux runoff response distribution to rainfall in panels **(e)** and **(f)**, which show similar temporal runoff response distributions when the response is averaged across the entire observation period rather than separated for times when active layer detachments are actively eroding the catchment (Fig. 7). Error bars indicate one standard error.

2008). More recent work has further demonstrated how seasonal active-layer thaw interacts with discharge and catchment characteristics to regulate stream chemistry across permafrost catchments (Grewal et al., 2025).

Figure 9 builds on an established conceptual foundation by explicitly linking the seasonal evolution of thaw and connectivity to event-scale runoff of water and material flux responses to rainfall, and illustrates how they manifest in the magnitude, timing, and persistence of rainfall-driven responses observed in our data, as quantified using ERRA. The conceptual model synthesizes three controls on rainfall-runoff behavior identified in this study: (1) seasonal changes in subsurface storage associated with active-layer development, (2) variations in antecedent effective wetness and hydrologic connectivity, and (3) geomorphic disturbance associated with active layer detachments. Together, these controls regulate both the magnitude of runoff response to rainfall and the mobilization of dissolved and particulate materials.

The processes summarized in Fig. 9 provide a framework for anticipating future shifts in rainfall-runoff behavior and, when combined with projections of precipitation change, warming temperatures, and evolving erosional processes, offer insight into potential hydrologic responses of permafrost catchments to climate change. Arctic climate projections anticipate both increased precipitation and warmer temperatures (Tebaldi et al., 2006; Bintanja et al., 2020). In Alaska, precipitation is expected to increase by 14 %–25 % between 2020 and 2049 (Bieniek et al., 2022; Bintanja et al., 2020), with most of the increase occurring as summer rainfall, given that snowfall is not projected to change significantly (Bintanja and Andry, 2017). Average winter temperatures are anticipated to rise by 3 °C over the next three decades (Bigalke and Walsh, 2022). Figure 5 suggests that it will be difficult to predict the net effect of these two trends, because their influences are similar (e.g., z-scores of 0.66 vs. 0.46 in Eq. 2), but have opposite effects on runoff sensitivity to rainfall. Because increased precipitation and warmer temperatures exert opposing influences on runoff sensitivity, the net hydrologic response to climate change remains uncertain. Future runoff behavior will likely depend on the balance between increasing rainfall inputs, evolving subsurface storage capacity, and changes in hydrologic connectivity and geomorphic disturbance.

In addition to rainfall and temperature increases, permafrost thaw will likely intensify erosional activity such as ALDs and lead to higher runoff (Q, M) with precipitation

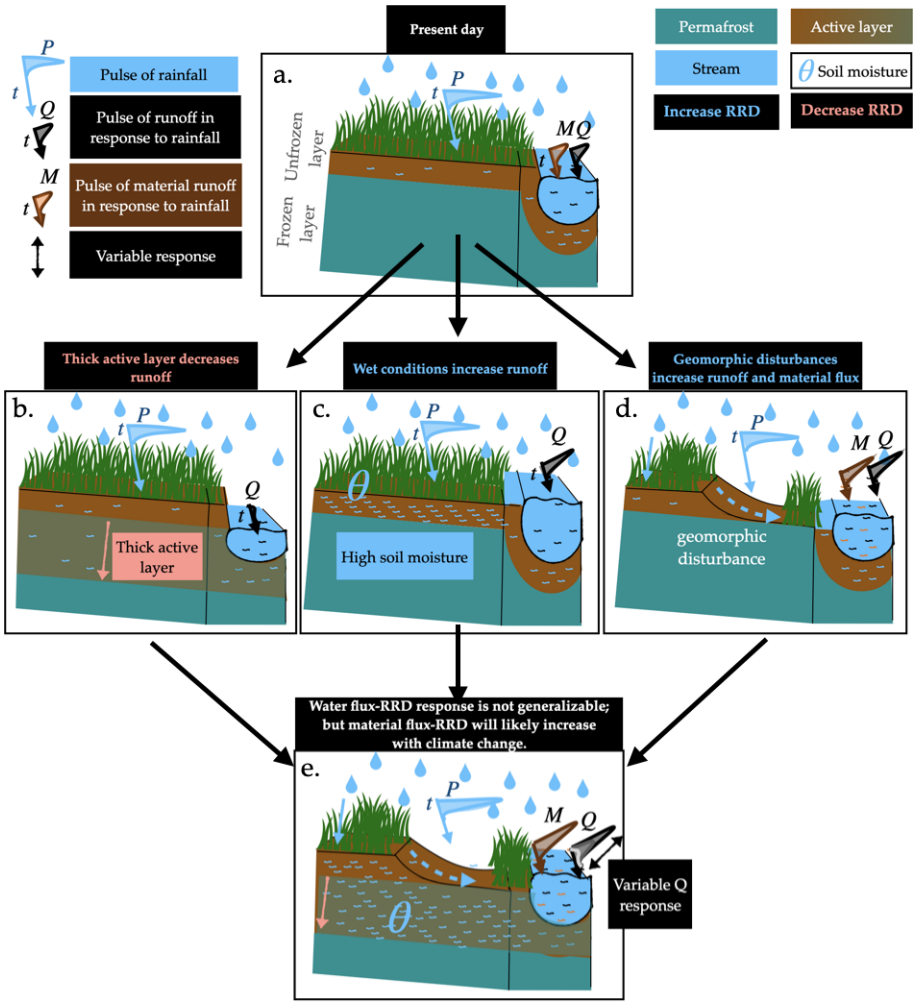


Figure 9. Conceptual model of processes influencing runoff response to rainfall in permafrost catchments. **(a)** A conceptual model of the present day conditions at a landscape underlain by permafrost. The model shows a cross section of a catchment that has an active layer (brown) over permafrost (turquoise). Panel **(a)** shows the present day material and water flux in response to a unit pulse of rainfall. As shown in the top left legend, arrows with a curve indicate the time (t) dependent component of rainfall (P) and runoff (Q, M). The blue curved arrow is to show a unit pulse of rainfall. The brown and black curved arrows are to show water (Q) and material (M) flux runoff response, respectively, to a unit pulse of rainfall. The height of the curve indicates the respective intensity of rainfall or the intensity of runoff response. **(b–d)** Panels **(b)–(d)** summarize how runoff response may vary based on our results. **(e)** These competing and interactive controls, considered alongside a future in which some regions will experience thicker active layers (pink arrow), increased rainfall (large curved blue arrow), and greater erosion, make it difficult to generalize climate-driven water-flux runoff trends. The double arrow line next to (1) the runoff response arrow and (2) the water levels show this variability in runoff response to different controls. We use different shades of gray about the runoff response arrow to illustrate the change in magnitude of the response. The label "Variable Q response" further highlights this variability. Regions that are prone to erosion by ALDs will see an increase in runoff of material fluxes with rainfall.

(Fig. 9d). One important implication of the enhanced runoff response associated with ALDs is the potential to increase risks of flash floods and damage to critical infrastructure. Numerous ALDs and retrogressive thaw slumps have occurred along major transportation corridors in Canada, Alaska, and the Tibetan Plateau, resulting in significant damage and road closures (e.g., Ackerson et al., 2021; Van der Sluijs et al., 2018; Luo et al., 2022). Beyond the direct infrastructure damage that such thaw features cause, they can also generate long-lasting risks to infrastructure by intensifying the flashiness of rainfall-runoff events.

Our results contribute to the ongoing discussion of how permafrost catchments are likely to respond to future climate changes. Beyond such generalized projections, however, our results can also inform year-by-year predictions based on expected weather conditions. For example, a wet summer following a cold winter is likely to yield strong runoff responses to rainfall. Similarly, a warm summer triggering ALDs may

further amplify those responses. This framework provides tangible insights into which years may experience hydrologic wetting or drying, offering a more actionable alternative to broad climate impact assessments in permafrost landscapes.

Code and data availability. The datasets and scripts used in this study are publicly available at https://doi.org/10.5281/zenodo.23171392 (Culha, 2026). This repository includes all code required to reproduce manuscript results, processed data for the Upper Kuparuk, Goose, and Ptarmigan catchments, and the main figures.

Supplement. The supplement related to this article is available online at https://doi.org/10.5194/hess-30-7177-2026-supplement.

Author contributions. CC and JWK contributed to conceptualization (formulation of research goals and aims) and methodology (development and design of methods, creation of models). CC carried out the formal analysis, investigation, writing – original draft preparation, and visualization. SG and ML were responsible for data curation. All authors contributed to writing – review and editing.

Competing interests. The contact author has declared that none of the authors has any competing interests.

Disclaimer. Publisher's note: Copernicus Publications remains neutral with regard to jurisdictional claims made in the text, published maps, institutional affiliations, or any other geographical representation in this paper. The authors bear the ultimate responsibility for providing appropriate place names. Views expressed in the text are those of the authors and do not necessarily reflect the views of the publisher.

Acknowledgements. The authors gratefully acknowledge the researchers, field technicians, and staff who have contributed to the long-term collection and maintenance of hydrological, meteorological, and biogeochemical datasets at the Upper Kuparuk River and Cape Bounty Arctic Watershed Observatory. We thank Toolik Field Station and the University of Alaska Fairbanks Water and Environmental Research Center for their contributions to the Upper Kuparuk observational record. We also thank the Cape Bounty Arctic Watershed Observatory research team and the Polar Continental Shelf Program for their sustained field and logistical support, as well as the community of Resolute and the Nunavut Research Institute for their support of research activities in the Canadian High Arctic. Finally, we acknowledge PermafrostNet for fostering scientific collaboration and knowledge exchange through conferences and research gatherings.

Financial support. CC received funding from the National Science Foundation through the EAR Postdoctoral Fellowship Program.

Review statement. This paper was edited by Markus Hrachowitz and reviewed by two anonymous referees.

References

Ackerson, C. M., Ward, B., and Kennedy, K.: Surficial geological mapping of the central Kluane Ranges (parts of NTS 115G/1, 2, 3, 7 and 115B/15, 16), southwestern Yukon, in: Yukon Exploration and Geology 2020, edited by: MacFarlane, K. E., Yukon Geological Survey, Whitehorse, Yukon, Canada, 157–176, https://emrlibrary.gov.yk.ca/ygs/yeg/2020/8_Ackerson_etal.pdf (last access: 20 October 2026), 2021.

Arp, C., Kane, D. L., Stuefer, S., and Hinzman, L.: Hydrographic data, Upper Kuparuk River watershed, Alaska, 1993–2017, Arctic Data Center [data set], https://doi.org/10.18739/A2WH2DD7W, 2017.

Arp, C. D., Jones, B. M., Liljedahl, A. K., Hinkel, K. M., and Welker, J. A.: Depth, ice thickness, and ice-out timing cause divergent hydrologic responses among Arctic lakes, Water Resour. Res., 51, 9379–9401, 2015.

Beel, C., Lamoureux, S., and Orwin, J.: Fluvial response to a period of hydrometeorological change and landscape disturbance in the Canadian High Arctic, Geophys. Res. Lett., 45, 10446–10456, https://doi.org/10.1029/2018GL079660, 2018.

Beel, C., Lamoureux, S., Orwin, J., Pope, M., Lafrenière, M., and Scott, N.: Differential impact of thermal and physical permafrost disturbances on High Arctic dissolved and particulate fluvial fluxes, Sci. Rep., 10, 11836, https://doi.org/10.1038/s41598-020-68824-3, 2020.

Beel, C., Heslop, J., Orwin, J., Pope, M., Schevers, A., Hung, J., Lafrenière, M., and Lamoureux, S.: Emerging dominance of summer rainfall driving High Arctic terrestrial-aquatic connectivity, Nat. Commun., 12, 1448, https://doi.org/10.1038/s41467-021-21759-3, 2021.

Beven, K. J.: Rainfall–Runoff Modelling: The Primer, 2nd edn., John Wiley and Sons, Chichester, UK, ISBN 978-0-470-71459-1, https://doi.org/10.1002/9781119951001, 2012.

Bieniek, P. A., Walsh, J. E., Fresco, N., Tauxe, C., and Redilla, K.: Anticipated changes in Alaska extreme precipitation, J. Appl. Meteorol. Clim., 61, 97–108, 2022.

Bigalke, S. and Walsh, J. E.: Future changes of snow in Alaska and the Arctic under stabilized global warming scenarios, Atmosphere, 13, 541, https://doi.org/10.3390/atmos13040541, 2022.

Bintanja, R. and Andry, O.: Towards a rain-dominated Arctic, Nat. Clim. Change, 7, 263–267, 2017.

Bintanja, R., van der Wiel, K., van der Linden, E., Reusen, J., Bogerd, L., Krikken, F., and Selten, F.: Strong future increases in Arctic precipitation variability linked to poleward moisture transport, Sci. Adv., 6, eaax6869, https://doi.org/10.1126/sciadv.aax6869, 2020.

Biskaborn, B. K., Smith, S. L., Noetzli, J., Matthes, H., Vieira, G., Streletskiy, D. A., Schoeneich, P., Romanovsky, V. E., Lewkowicz, A. G., Abramov, A., Allard, M., Boike, J., Cable, W. L., Christiansen, H. H., Delaloye, R., Diekmann, B., Drozdov, D., Etzelmüller, B., Grosse, G., Guglielmin, M., Ingeman-Nielsen, T., Isaksen, K., Ishikawa, M., Johansson, M., Johannsson, H., Joo, A., Kaverin, D., Kholodov, A., Konstantinov, P., Kröger, T., Lambiel, C., Lanckman, J.-P., Luo, D., Malkova, G., Meiklejohn,

I., Moskalenko, N., Oliva, M., Phillips, M., Ramos, M., Sannel, A. B. K., Sergeev, D., Seybold, C., Skryabin, P., Vasiliev, A., Wu, Q., Yoshikawa, K., Zheleznyak, M., and Lantuit, H.: Permafrost is warming at a global scale, Nat. Commun., 10, 264, https://doi.org/10.1038/s41467-018-08240-4, 2019.

Bowden, W. B., Gooseff, M. N., Balser, A., Green, A., Peterson, B. J., and Bradford, J.: Sediment and nutrient delivery from thermokarst features in the foothills of the North Slope, Alaska: Potential impacts on headwater stream ecosystems, J. Geophys. Res.-Biogeo., 113, https://doi.org/10.1029/2007JG000470, 2008.

Chen, S., Fu, Y. H., Geng, X., Hao, Z., Tang, J., Zhang, X., Xu, Z., and Hao, F.: Influences of shifted vegetation phenology on runoff across a hydroclimatic gradient, Front. Plant Sci., 12, 802664, https://doi.org/10.3389/fpls.2021.802664, 2022.

Coch, C., Lamoureux, S. F., Knoblauch, C., Eischeid, I., Fritz, M., Obu, J., and Lantuit, H.: Summer rainfall dissolved organic carbon, solute, and sediment fluxes in a small Arctic coastal catchment on Herschel Island (Yukon Territory, Canada), Arct. Sci., 4, 750–780, 2018.

Connon, R. F., Quinton, W. L., Craig, J. R., and Hayashi, M.: Changing hydrologic connectivity due to permafrost thaw in the lower Liard River valley, NWT, Canada, Hydrol. Process., 28, 4163–4178, 2014.

Cook, R. D. and Weisberg, S.: Residuals and Influence in Regression, Chapman and Hall, New York, USA, ISBN 978-0-412-24280-9, 1982.

Crowther, T. W., Todd-Brown, K. E. O., Rowe, C. W., Wieder, W. R., Carey, J. C., Machmuller, M. B., Snoek, B. L., Fang, S., Zhou, G., Allison, S. D., Blair, J. M., Bridgham, S. D., Burton, A. J., Carrillo, Y., Reich, P. B., Clark, J. S., Classen, A. T., Dijkstra, F. A., Elberling, B., Emmett, B. A., Estiarte, M., Frey, S. D., Guo, J., Harte, J., Jiang, L., Johnson, B. R., Kröel-Dulay, G., Larsen, K. S., Laudon, H., Lavallee, J. M., Luo, Y., Lupascu, M., Ma, L. N., Marhan, S., Michelsen, A., Mohan, J., Niu, S., Pendall, E., Peñuelas, J., Pfeifer-Meister, L., Poll, C., Reinsch, S., Reynolds, L. L., Schmidt, I. K., Sistla, S., Sokol, N. W., Templer, P. H., Treseder, K. K., Welker, J. M., and Bradford, M. A.: Quantifying global soil carbon losses in response to warming, Nature, 540, 104–108, 2016.

Culha, C.: Data and code for: Characterizing runoff response to rainfall in permafrost catchments and its implications for hydrological and biogeochemical fluxes in a warming climate (Version v1.0.0), Zenodo [data set] [code], https://doi.org/10.5281/zenodo.23171392, 2026.

DeBeer, C. M., Wheater, H. S., Carey, S. K., and Chun, K. P.: Recent climatic, cryospheric, and hydrological changes over the interior of western Canada: a review and synthesis, Hydrol. Earth Syst. Sci., 20, 1573–1598, https://doi.org/10.5194/hess-20-1573-2016, 2016.

Del Vecchio, J. and Evans, S. G.: Climate and hydrogeological controls on water tracks in permafrost landscapes, Rev. Geophys., 63, e2024RG000854, https://doi.org/10.1029/2024RG000854, 2025.

Déry, S. J., Crow, W. T., Stieglitz, M., and Wood, E. F.: Modeling snow-cover heterogeneity over complex Arctic terrain for regional and global climate models, J. Hydrometeorol., 5, 33–48, 2004.

Déry, S. J., Salomonson, V. V., Stieglitz, M., Hall, D. K., and Appel, I.: An approach to using snow areal depletion curves inferred from MODIS and its application to land surface modelling in Alaska, Hydrol. Process., 19, 2755–2774, 2005.

Dingman, S. L.: Hydrology of the Glenn Creek watershed, Tanana River basin, central Alaska, Research Report 297, U.S. Army Cold Regions Research and Engineering Laboratory, Hanover, NH, USA, 00204405, 111 pp., 1971.

Eschenfelder, J. A., Chartrand, S. M., Jellinek, A. M., and Culha, C.: Seasonal freezing increases High Arctic erosion and landscape response to climate extremes, Commun. Earth Environ., 7, 388, https://doi.org/10.1038/s43247-026-03468-1, 2026.

Evans, S. G., Godsey, S. E., Rushlow, C. R., and Voss, C.: Water tracks enhance water flow above permafrost in upland Arctic Alaska hillslopes, J. Geophys. Res.-Earth, 125, e2019JF005256, https://doi.org/10.1029/2019JF005256, 2020.

Favaro, E. A. and Lamoureux, S. F.: Antecedent controls on rainfall runoff response and sediment transport in a High Arctic catchment, Geogr. Ann. A, 96, 433–446, https://doi.org/10.1111/geoa.12063, 2014.

Fouché, J., Lafrenière, M. J., Rutherford, K., and Lamoureux, S.: Seasonal hydrology and permafrost disturbance impacts on dissolved organic matter composition in High Arctic headwater catchments, Arct. Sci., 3, 378–405, 2017.

Frampton, A. and Destouni, G.: Impact of degrading permafrost on subsurface solute transport pathways and travel times, Water Resour. Res., 51, 7680–7701, 2015.

Frey, K. E. and McClelland, J. W.: Impacts of permafrost degradation on Arctic river biogeochemistry, Hydrol. Process., 23, 169–182, 2009.

Genxu, W., Tianxu, M., Juan, C., Chunlin, S., and Kewei, H.: Processes of runoff generation operating during the spring and autumn seasons in a permafrost catchment on semi-arid plateaus, J. Hydrol., 550, 307–317, 2017.

Gooseff, M. N., Balser, A., Bowden, W. B., and Jones, J. B.: Effects of hillslope thermokarst in northern Alaska, Eos Trans. AGU, 90, 29–30, 2009.

Grewal, A., Nicholls, E. M., and Carey, S. K.: The role of catchment characteristics, discharge, and active- layer thaw in seasonal stream chemistry across 10 permafrost catchments, Hydrol. Earth Syst. Sci., 29, 2467–2483, https://doi.org/10.5194/hess-29-2467-2025, 2025.

Hamm, A. and Frampton, A.: Impact of lateral groundwater flow on hydrothermal conditions of the active layer in a high-Arctic hillslope setting, The Cryosphere, 15, 4853–4871, https://doi.org/10.5194/tc-15-4853-2021, 2021.

Helbig, M., Waddington, J. M., Alekseychik, P., Amiro, B. D., Aurela, M., Barr, A. G., Black, T. A., Blanken, P. D., Carey, S. K., Chen, J., Chi, J., Desai, A. R., Dunn, A., Euskirchen, E. S., Flanagan, L. B., Forbrich, I., Friborg, T., Grelle, A., Harder, S., Heliasz, M., Humphreys, E. R., Ikawa, H., Isabelle, P.-E., Iwata, H., Jassal, R., Korkiakoski, M., Kurbatova, J., Kutzbach, L., Lindroth, A., Löfvenius, M. O., Lohila, A., Mammarella, I., Marsh, P., Maximov, T., Melton, J. R., Moore, P. A., Nadeau, D. F., Nicholls, E. M., Nilsson, M. B., Ohta, T., Peichl, M., Petrone, R. M., Petrov, R., Prokushkin, A., Quinton, W. L., Reed, D. E., Roulet, N. T., Runkle, B. R. K., Sonnentag, O., Strachan, I. B., Taillardat, P., Tuittila, E.-S., Tuovinen, J.-P., Turner, J., Ueyama, M., Varlagin, A., Wilmking, M., Wofsy, S. C., and Zyrianov, V.:

Increasing contribution of peatlands to boreal evapotranspiration in a warming climate, Nat. Clim. Change, 10, 555–560, 2020.

Hinzman, L. D., Kane, D. L., Gieck, R. E., and Everett, K. R.: Hydrologic and thermal properties of the active layer in the Alaskan Arctic, Cold Reg. Sci. Technol., 19, 95–110, 1991.

Jan, A. and Painter, S. L.: Permafrost thermal conditions are sensitive to shifts in snow timing, Environ. Res. Lett., 15, 084026, https://doi.org/10.1088/1748-9326/ab8ec4, 2020.

Jan, A., Coon, E. T., and Painter, S. L.: Evaluating integrated surface/subsurface permafrost thermal hydrology models in ATS (v0.88) against observations from a polygonal tundra site, Geosci. Model Dev., 13, 2259–2276, 2020.

Jorgenson, K. L., Douglas, T. A., Jorgenson, M. T., Pastick, N. J., and Harms, T. K.: Permafrost and Rain Influence Summer Hydrologic Flowpaths in Boreal Catchments, Water Resour. Res., 61, e2024WR039024, https://doi.org//10.1029/2024WR039024, 2025.

Jorgenson, M. T., Romanovsky, V., Harden, J., Shur, Y., O'Donnell, J., Schuur, E. A. G., Kanevskiy, M., and Marchenko, S.: Resilience and vulnerability of permafrost to climate change, Can. J. Forest Res., 40, 1219–1236, 2010.

Kane, D. L., Hinzman, L., McNamara, J., Zhang, Z., and Benson, C.: An overview of a nested watershed study in Arctic Alaska, Nord. Hydrol., 31, 245–266, 2000.

Kane, D. L., Hinzman, L. D., Yang, D., Galloway, J. M., and Benson, C. S.: Contrasting extreme runoff events in areas of continuous permafrost, North Slope of Alaska, Hydrol. Res., 39, 287–298, 2008.

Kane, D. L., Hinzman, L., Stuefer, S., and Arp, C.: Updated meteorological, radiation, and soil temperature data, Kuparuk River and nearby watersheds: Upper Kuparuk (UK) station, 1994–2018, Arctic Data Center [data set], https://doi.org/10.18739/A29P2W70H, 2021.

Kirchner, J. W.: Impulse response functions for nonlinear, nonstationary, and heterogeneous systems, estimated by deconvolution and demixing of noisy time series, Sensors, 22, 3291, https://doi.org/10.3390/s22093291, 2022.

Kirchner, J. W.: Characterizing nonlinear, nonstationary, and heterogeneous hydrologic behavior using ensemble rainfall–runoff analysis (ERRA): proof of concept, Hydrol. Earth Syst. Sci., 28, 4427–4454, https://doi.org/10.5194/hess-28-4427-2024, 2024.

Knapp, J. L. A., Berghuijs, W. R., Floriancic, M. G., and Kirchner, J. W.: Catchment hydrological response and transport are affected differently by precipitation intensity and antecedent wetness, Hydrol. Earth Syst. Sci., 29, 3673–3685, https://doi.org/10.5194/hess-29-3673-2025, 2025.

Koch, J. C., Dornblaser, M. M., and Striegl, R. G.: Storm-scale and seasonal dynamics of carbon export from a nested subarctic watershed underlain by permafrost, J. Geophys. Res.-Biogeo., 126, e2021JG006268, https://doi.org/10.1029/2021JG006268, 2021.

Kokelj, S. V., Lacelle, D., Lantz, T. C., Tunnicliffe, J., Malone, L., Clark, I. D., and Chin, K. S.: Thawing of massive ground ice in mega slumps drives increases in stream sediment and solute flux across a range of watershed scales, J. Geophys. Res.-Earth, 118, 681–692, 2013.

Kokelj, S. V., Lantz, T. C., Tunnicliffe, J., Segal, R., and Lacelle, D.: Climate-driven thaw of permafrost preserved glacial landscapes, northwestern Canada, Geology, 45, 371–374, 2017.

Kokelj, S. V., Kokoszka, J., van der Sluijs, J., Rudy, A. C. A., Tunnicliffe, J., Shakil, S., Tank, S. E., and Zolkos, S.: Thaw-driven mass wasting couples slopes with downstream systems, and effects propagate through Arctic drainage networks, The Cryosphere, 15, 3059–3081, https://doi.org/10.5194/tc-15-3059-2021, 2021.

Kokelj, S. V., Gingras-Hill, T., Daly, S. V., Morse, P. D., Wolfe, S. A., Rudy, A. C. A., van der Sluijs, J., Weiss, N., O'Neill, H. B., Baltzer, J. L., Lantz, T. C., Gibson, C., Cazon, D., Fraser, R. H., Froese, D. G., Giff, G., Klengenberg, C., Lamoureux, S. F., Quinton, W. L., Turetsky, M. R., Chiasson, A., Ferguson, C., Newton, M., Pope, M., Paul, J. A., Wilson, A., and Young, J. M.: The Northwest Territories Thermokarst Mapping Collective: A northern-driven mapping collaborative toward understanding the effects of permafrost thaw, Arct. Sci., 9, 886–918, 2023.

Kokelj, S. V., Wolfe, S. A., Weiss, N., Froese, D., Baltzer, J. L., Lantz, T. C., O'Neill, H. B., Morse, P. D., Sniderhan, A., Speetjens, N. J., van der Sluijs, J., Alvarez, A., Tank, S. E., and Gruber, S.: Permafrost landsystems define regional variability in climate change effects on northern environments, Nat. Commun., 17, 4799, https://doi.org/10.1038/s41467-026-71216-2, 2026.

Kurylyk, B. L. and Watanabe, K.: The mathematical representation of freezing and thawing processes in variably-saturated, non-deformable soils, Adv. Water Resour., 60, 160–177, 2013.

Lafrenière, M. J. and Lamoureux, S. F.: Effects of changing permafrost conditions on hydrological processes and fluvial fluxes, Earth-Sci. Rev., 191, 212–223, 2019.

Lamoureux, S. F. and Lafrenière, M. J.: Fluvial impact of extensive active layer detachments, Cape Bounty, Melville Island, Canada, Arct. Antarct. Alp. Res., 41, 59–68, https://doi.org/10.1657/1523-0430-41.1.59, 2009.

Lamoureux, S. F. and Lafrenière, M. J.: Seasonal fluxes and age of particulate organic carbon exported from Arctic catchments impacted by localized permafrost slope disturbances, Environ. Res. Lett., 9, 045002, https://doi.org/10.1088/1748-9326/9/4/045002, 2014.

Lamoureux, S. F., Lafrenière, M. J., and Favaro, E. A.: Erosion dynamics following localized permafrost slope disturbances, Geophys. Res. Lett., 41, 5499–5505, 2014.

Levy, J. S., Fountain, A. G., Gooseff, M. N., Welch, K. A., and Lyons, W. B.: Water tracks and permafrost in Taylor Valley, Antarctica: Extensive and shallow groundwater connectivity in a cold desert ecosystem, Geol. Soc. Am. Bull., 123, 2295–2311, https://doi.org/10.1130/B30436.1, 2011.

Liljedahl, A. K., Hinzman, L. D., Harazono, Y., Zona, D., Tweedie, C. E., Hollister, R. D., Engstrom, R., and Oechel, W. C.: Nonlinear controls on evapotranspiration in Arctic coastal wetlands, Biogeosciences, 8, 3375–3389, 2011.

Liljedahl, A. K., Boike, J., Daanen, R. P., Fedorov, A. N., Frost, G. V., Grosse, G., Hinzman, L. D., Iijma, Y., Jorgenson, J. C., Matveyeva, N., Necsoiu, M., Raynolds, M. K., Romanovsky, V. E., Schulla, J., Tape, K. D., Walker, D. A., Wilson, C. J., Yabuki, H., and Zona, D.: Pan-Arctic ice-wedge degradation in warming permafrost and its influence on tundra hydrology, Nat. Geosci., 9, 312–318, 2016.

Luo, J., Niu, F., Lin, Z., Liu, M., Yin, G., and Gao, Z.: Inventory and frequency of retrogressive thaw slumps in the permafrost region of the Qinghai–Tibet Plateau, Geophys. Res. Lett., 49, e2022GL099829, https://doi.org/10.1029/2022GL099829, 2022.

Massari, C., Pellet, V., Tramblay, Y., Crow, W. T., Gründemann, G. J., Hascoet, T., Penna, D., Modanesi, S., Brocca, L., Camici, S., and Marra, F.: On the relation between antecedent basin conditions and runoff coefficient for European floods, J. Hydrol., 625, 130012, https://doi.org/10.1016/j.jhydrol.2023.130012, 2023.

McNamara, J. P., Kane, D. L., and Hinzman, L. D.: Hydrograph separations in an Arctic watershed using mixing model and graphical techniques, Water Resour. Res., 33, 1707–1719, 1997.

McNamara, J. P., Kane, D. L., and Hinzman, L. D.: An analysis of streamflow hydrology in the Kuparuk River Basin, Arctic Alaska: a nested watershed approach, J. Hydrol., 206, 39–57, https://doi.org/10.1016/S0022-1694(98)00083-3, 1998.

McNamara, J. P., Kane, D. L., and Hinzman, L. D.: An analysis of an Arctic channel network using a digital elevation model, Geomorphology, 29, 339–353, 1999.

Mekis, E. and Hogg, W. D.: Rehabilitation and analysis of Canadian daily precipitation time series, Atmos. Ocean, 37, 53–85, 1999.

Neilson, B. T., Cardenas, M. B., O'Connor, M. T., Rasmussen, M. T., King, T. V., and Kling, G. W.: Groundwater flow and exchange across the land surface explain carbon export patterns in continuous permafrost watersheds, Geophys. Res. Lett., 45, 7596–7605, 2018.

Nelson, F., Shiklomanov, N., Mueller, G., Hinkel, K., Walker, D., and Bockheim, J.: Estimating active-layer thickness over a large region: Kuparuk River basin, Alaska, USA, Arctic Alpine Res., 29, 367–378, 1997.

O'Connor, M. T., Cardenas, M. B., Ferencz, S. B., Wu, Y., Neilson, B. T., Chen, J., and Kling, G. W.: Empirical models for predicting water and heat flow properties of permafrost soils, Geophys. Res. Lett., 47, e2020GL087646, https://doi.org/10.1029/2020GL087646, 2020.

Painter, S. L., Moulton, J. D., and Wilson, C. J.: Modeling challenges for predicting hydrologic response to degrading permafrost, Hydrogeol. J., 21, 221–224, 2013.

Painter, S. L., Coon, E. T., Atchley, A. L., Berndt, M., Garimella, R., Moulton, J. D., Svyatskiy, D., and Wilson, C. J.: Integrated surface/subsurface permafrost thermal hydrology: Model formulation and proof-of-concept simulations, Water Resour. Res., 52, 6062–6077, 2016.

Painter, S. L., Coon, E. T., Khattak, A. J., and Jastrow, J. D.: Drying of tundra landscapes will limit subsidence-induced acceleration of permafrost thaw, P. Natl. Acad. Sci. USA, 120, e2212171120, https://doi.org/10.1073/pnas.2212171120, 2023.

Paquette, M., Rudy, A. C., Fortier, D., and Lamoureux, S. F.: Multi-scale site evaluation of a relict active layer detachment in a High Arctic landscape, Geomorphology, 359, 107159, https://doi.org/10.1016/j.geomorph.2020.107159, 2020.

Porter, C., Morin, P., Howat, I., Noh, M.-J., Bates, B., Peterman, K., Keesey, S., Schlenk, M., Gardiner, J., Tomko, K., Willis, M., Kelleher, C., Cloutier, M., Husby, E., Foga, S., Nakamura, H., Platson, M., Wethington, M., Williamson, C., Bauer, G., Enos, J., Arnold, G., Kramer, W., Becker, P., Doshi, A., D'Souza, C., Cummens, P., Laurier, F., and Bojesen, M.: ArcticDEM, Version 3, Harvard Dataverse [data set], https://doi.org/10.7910/DVN/OHHUKH, 2018.

Qin, J., Yang, B., Ding, Y., Cui, J., and Zhang, Y.: Assessment of runoff generation capacity and total runoff contribution for different landscapes in alpine and permafrost watershed, Catena, 249, 108643, https://doi.org/10.1016/j.catena.2024.108643, 2025.

Quinton, W. L. and Carey, S. K.: Towards an energy-based runoff generation theory for tundra landscapes, Hydrol. Process., 22, 4649–4653, 2008.

Quinton, W. L. and Marsh, P.: A conceptual framework for runoff generation in a permafrost environment, Hydrol. Process., 13, 2563–2581, 1999.

Quinton, W. L., Gray, D. M., and Marsh, P.: Subsurface drainage from hummock-covered hillslopes in the Arctic tundra, J. Hydrol., 237, 113–125, 2000.

Quinton, W. L., Bemrose, R. K., Zhang, Y., and Carey, S. K.: The influence of spatial variability in snowmelt and active layer thaw on hillslope drainage for an alpine tundra hillslope, Hydrol. Process., 23, 2628–2639, 2009.

Rawlins, M. A. and Karmalkar, A. V.: Regime shifts in Arctic terrestrial hydrology manifested from impacts of climate warming, The Cryosphere, 18, 1033–1052, https://doi.org/10.5194/tc-18-1033-2024, 2024.

Rawlins, M. A., Connolly, C. T., and McClelland, J. W.: Modeling terrestrial dissolved organic carbon loading to western Arctic rivers, J. Geophys. Res.-Biogeo., 126, e2021JG006420, https://doi.org//10.1029/2021JG006420, 2021.

Rushlow, C. R. and Godsey, S. E.: Rainfall–runoff responses on Arctic hillslopes underlain by continuous permafrost, North Slope, Alaska, USA, Hydrol. Process., 31, 4092–4106, 2017.

Scherler, M., Hauck, C., Hoelzle, M., Stähli, M., and Völksch, I.: Meltwater infiltration into the frozen active layer at an alpine permafrost site, Permafrost Periglac., 21, 325–334, 2010.

Shiklomanov, N.: Toolik MAT: Active layer thickness grid measurements at Toolik, Alaska (site ID: 229), Circumpolar Active Layer Monitoring (CALM) program, The George Washington University [data set], http://gtnpdatabase.org/activelayers/view/229 (last access: 30 January 2024), 2014.

Shogren, A. J., Zarnetske, J. P., Abbott, B. W., Iannucci, F., Frei, R. J., Griffin, N. A., and Bowden, W. B.: Revealing biogeochemical signatures of Arctic landscapes with river chemistry, Sci. Rep., 9, 12894, https://doi.org/10.1038/s41598-019-49296-6, 2019.

Shogren, A. J., Zarnetske, J. P., Abbott, B. W., Bratsman, S., Brown, B., Carey, M. P., Fulweber, R., Greaves, H. E., Haines, E., Iannucci, F., Koch, J. C., Medvedeff, A., O'Donnell, J. A., Patch, L., Poulin, B. A., Williamson, T. J., and Bowden, W. B.: Multi-year, spatially extensive, watershed-scale synoptic stream chemistry and water quality conditions for six permafrost-underlain Arctic watersheds, Earth Syst. Sci. Data, 14, 95–116, https://doi.org/10.5194/essd-14-95-2022, 2022.

Shogren, A. J., Zarnetske, J. P., Abbott, B. W., Grose, A. L., Rec, A. F., Nipko, J., Song, C., O'Donnell, J. A., and Bowden, W. B.: Hydrology controls dissolved organic carbon and nitrogen export and post-storm recovery in two Arctic headwaters, J. Geophys. Res.-Biogeo., 129, e2023JG007583, https://doi.org/10.1029/2023JG007583, 2024.

Sjöberg, Y., Jan, A., Painter, S. L., Coon, E. T., Carey, M. P., O'Donnell, J. A., and Koch, J. C.: Permafrost promotes shallow groundwater flow and warmer headwater streams, Water Resour. Res., 57, e2020WR027463, https://doi.org/10.1029/2020WR027463, 2021.

Smith, L. C., Pavelsky, T. M., MacDonald, G. M., Shiklomanov, A. I., and Lammers, R. B.: Rising minimum daily flows in north-

ern Eurasian rivers: A growing influence of groundwater in the high-latitude hydrologic cycle, J. Geophys. Res.-Biogeo., 112, https://doi.org/10.1029/2006JG000327, 2007.

Spence, C., Kokelj, S. V., Kokelj, S. A., McCluskie, M., and Hedstrom, N.: Evidence of a change in water chemistry in Canada's subarctic associated with enhanced winter streamflow, J. Geophys. Res.-Biogeo., 120, 113–127, https://doi.org/10.1002/2014JG002809, 2015.

St. Jacques, J.-M. and Sauchyn, D. J.: Increasing winter baseflow and mean annual streamflow from possible permafrost thawing in the Northwest Territories, Canada, Geophys. Res. Lett., 36, https://doi.org/10.1029/2008GL035822, 2009.

Stähli, M., Jansson, P.-E., and Lundin, L.-C.: Soil moisture redistribution and infiltration in frozen sandy soils, Water Resour. Res., 35, 95–103, 1999.

Stieglitz, M., Shaman, J., McNamara, J., Engel, V., Shanley, J., and Kling, G. W.: An approach to understanding hydrologic connectivity on the hillslope and the implications for nutrient transport, Global Biogeochem. Cy., 17, https://doi.org/10.1029/2003GB002041, 2003.

Tank, S. E., Striegl, R. G., McClelland, J. W., and Kokelj, S. V.: Multi-decadal increases in dissolved organic carbon and alkalinity flux from the Mackenzie drainage basin to the Arctic Ocean, Environ. Res. Lett., 11, 054015, https://doi.org/10.1088/1748-9326/11/5/054015, 2016.

Tank, S. E., Vonk, J. E., Walvoord, M. A., McClelland, J. W., Laurion, I., and Abbott, B. W.: Landscape matters: Predicting the biogeochemical effects of permafrost thaw on aquatic networks with a state factor approach, Permafrost Periglac., 31, 358–370, 2020.

Tank, S. E., McClelland, J. W., Spencer, R. G. M., Shiklomanov, A. I., Suslova, A., Moatar, F., Amon, R. M. W., Cooper, L. W., Elias, G., Gordeev, V. V., Guay, C., Gurtovaya, T. Y., Kosmenko, L. S., Mutter, E. A., Peterson, B. J., Peucker-Ehrenbrink, B., Raymond, P. A., Schuster, P. F., Scott, L., Staples, R., Striegl, R. G., Tretiakov, M., Zhulidov, A. V., Zimov, N., Zimov, S., and Holmes, R. M.: Recent trends in the chemistry of major northern rivers signal widespread Arctic change, Nat. Geosci., 16, 789–796, 2023.

Tebaldi, C., Hayhoe, K., Arblaster, J. M., and Meehl, G. A.: Going to the extremes: an intercomparison of model-simulated historical and future changes in extreme events, Climatic Change, 79, 185–211, 2006.

Toohey, R. C., Herman-Mercer, N. M., Schuster, P. F., Mutter, E. A., and Koch, J. C.: Multidecadal increases in the Yukon River Basin of chemical fluxes as indicators of changing flowpaths, groundwater, and permafrost, Geophys. Res. Lett., 43, 12120–12130, https://doi.org/10.1002/2016GL070817, 2016.

Van der Sluijs, J., Kokelj, S. V., Fraser, R. H., Tunnicliffe, J., and Lacelle, D.: Permafrost terrain dynamics and infrastructure impacts revealed by UAV photogrammetry and thermal imaging, Remote Sens., 10, 1734, https://doi.org/10.3390/rs10111734, 2018.

van Everdingen, R. (Ed.): Multi-language glossary of permafrost and related ground-ice terms in Chinese, English, French, German, International Permafrost Association, Arctic Institute of North America, University of Calgary, Calgary, Canada, https://www.permafrost.org/wp-content/uploads/Glossary/Glossary_of_Permafrost_and_Related_Ground-Ice_Terms_1998.pdf (last access: 20 October 2026), 1998.

Velicogna, I., Tong, J., Zhang, T., and Kimball, J. S.: Increasing subsurface water storage in discontinuous permafrost areas of the Lena River basin, Eurasia, detected from GRACE, Geophys. Res. Lett., 39, https://doi.org/10.1029/2012GL051623, 2012.

Walvoord, M. A. and Kurylyk, B. L.: Hydrologic impacts of thawing permafrost – a review, Vadose Zone J., 15, 1–20, https://doi.org/10.2136/vzj2016.01.0010, 2016.

Walvoord, M. A. and Striegl, R. G.: Increased groundwater to stream discharge from permafrost thawing in the Yukon River basin: Potential impacts on lateral export of carbon and nitrogen, Geophys. Res. Lett., 34, https://doi.org/10.1029/2007GL030216, 2007.

Wang, K., Zhang, T., and Yang, D.: Permafrost dynamics and their hydrologic impacts over the Russian Arctic drainage basin, Adv. Clim. Change Res., 12, 482–498, 2021a.

Wang, P., Huang, Q., Pozdniakov, S. P., Liu, S., Ma, N., Wang, T., Zhang, Y., Yu, J., Xie, J., Fu, G., Frolova, N. L., and Liu, C.: Potential role of permafrost thaw on increasing Siberian river discharge, Environ. Res. Lett., 16, 034046, https://doi.org/10.1088/1748-9326/abe326, 2021b.

Woo, M. and Steer, P.: Occurrence of surface flow on Arctic slopes, southwestern Cornwallis Island, Can. J. Earth Sci., 19, 2368–2377, https://doi.org/10.1139/e82-206, 1982.

Woo, M.-K., Marsh, P., and Pomeroy, J. W.: Snow, frozen soils and permafrost hydrology in Canada, 1995–1998, Hydrol. Process., 14, 1591–1611, 2000.

Xiao, X., Liu, Z., Liu, K., and Wang, J.: Temporal variation of suspended sediment and solute fluxes in a permafrost-underlain headwater catchment on the Tibetan Plateau, Water, 14, 2782, https://doi.org/10.3390/w14182782, 2022.

Youcha, E. and Stuefer, S.: Arctic hydrology: a water balance study of Imnavait Creek and Kuparuk River watersheds, Alaska, Arct. Sci., 12, 1–30, https://doi.org/10.1139/as-2025-0033, 2026.